



Nanocrystalline diamond

O.A. Williams ^{*,1}

Fraunhofer Institute for Applied Solid State Physics, Tullastraße 72, 79108 Freiburg, Germany

ARTICLE INFO

Article history:

Received 17 November 2010
 Received in revised form 17 February 2011
 Accepted 23 February 2011
 Available online 9 March 2011

Keywords:

Nanocrystalline
 Chemical vapour deposition
 Nanostructures
 Diamond

ABSTRACT

Diamond properties are significantly affected by crystallite size. High surface to volume fractions result in enhanced disorder, sp^2 bonding, hydrogen content and scattering of electrons and phonons. Most of these properties are common to all low dimensional materials, but the addition of carbon allotropes introduces sp^2 bonding, a significant disadvantage over systems such as amorphous silicon. Increased sp^2 bonding results in enhanced disorder, a significantly more complex density of states within the bandgap, reduction of Young's modulus, increased optical absorption etc. At sizes below 10 nm, many diamond particle and film properties deviate substantially from that of bulk diamond, mostly due not only to the contribution of sp^2 bonding, but also at the extreme low dimensions due to size effects. Despite these drawbacks, nano-diamond films and particles are powerful systems for a variety of applications and the study of fundamental science. Knowledge of the fundamental properties of these materials allows a far greater exploitation of their attributes for specific applications. This review attempts to guide the reader between the various nanocrystalline diamond forms and applications, with a particular focus on thin films grown by chemical vapour deposition.

© 2011 Elsevier B.V. All rights reserved.

Contents

1.	Introduction	621
2.	Surface to volume ratio	622
3.	Nucleation	623
3.1.	Mechanical abrasion techniques (scratching)	624
3.2.	Ultrasonic particle treatment (micro-chipping)	625
3.3.	Carbon, carbide and carbide forming interlayers	625
3.4.	Bias enhanced nucleation	625
3.5.	Seeding with diamond nano-particles	626
3.6.	Combinatorial approaches	626
4.	Growth and morphology	626
4.1.	Incubation period	626
4.2.	Suppression/enhancement of re-nucleation processes	627
4.3.	Growth techniques	628
4.4.	Grain size/surface to volume ratio, sp^2 and hydrogen content	630
4.5.	Low temperature growth	633
5.	Thermal conductivity and Young's modulus	635
6.	Optical and electronic properties	635
7.	Applications	637
8.	Conclusions	638
	References	638

1. Introduction

Diamond films and particles are interesting in both fundamental and applied sciences due to their extreme and in many cases superlative properties. In fact, despite huge research efforts in the other allotropes and forms of carbon such as C_{60} , carbon nanotubes and graphene,

* Tel.: +49 761 5159 263.

E-mail address: oliverwilliams@mac.com.

¹ Now at: Cardiff School of Physics and Astronomy, Cardiff University, Queens Buildings, The Parade, Cardiff, CF24 3AA, United Kingdom.

diamond and graphite remain the most successful commercially exploited allotropes to date. The overwhelming majority of these applications are passive, such as cutting tools, abrasives, thermal management etc., not to mention the gem industry. Many of these application areas have been satisfied by natural diamond and diamond grown via High Pressure High Temperature (HPHT) synthesis, but the advent of Chemical Vapour Deposition (CVD) has led to a far wider circle of applications and an increase in the sophistication of diamond technologies. Principally, CVD allows the deposition of diamond on foreign substrates and the production of large areas for heat spreading, laser/extreme environment windows etc. Thus CVD and HPHT synthetic diamonds have become high tech products as a bulk material of extreme performance. Unfortunately, the lack of suitable dopants for electronic applications, led to a marked reduction of interest in CVD diamond research from the end of the 20th century.

Nano-structured diamond has rekindled much of this interest, offering many bulk diamond properties in a thin film package or small particle form. Fig. 1 shows the number of publications and citations of publications with the topic of nanocrystalline diamond. It can be seen that the field is booming and shows no sign of slowing down. As this review was being written there were over 22,000 citations in this topic over the last 20 years alone, excluding those under nanodia-

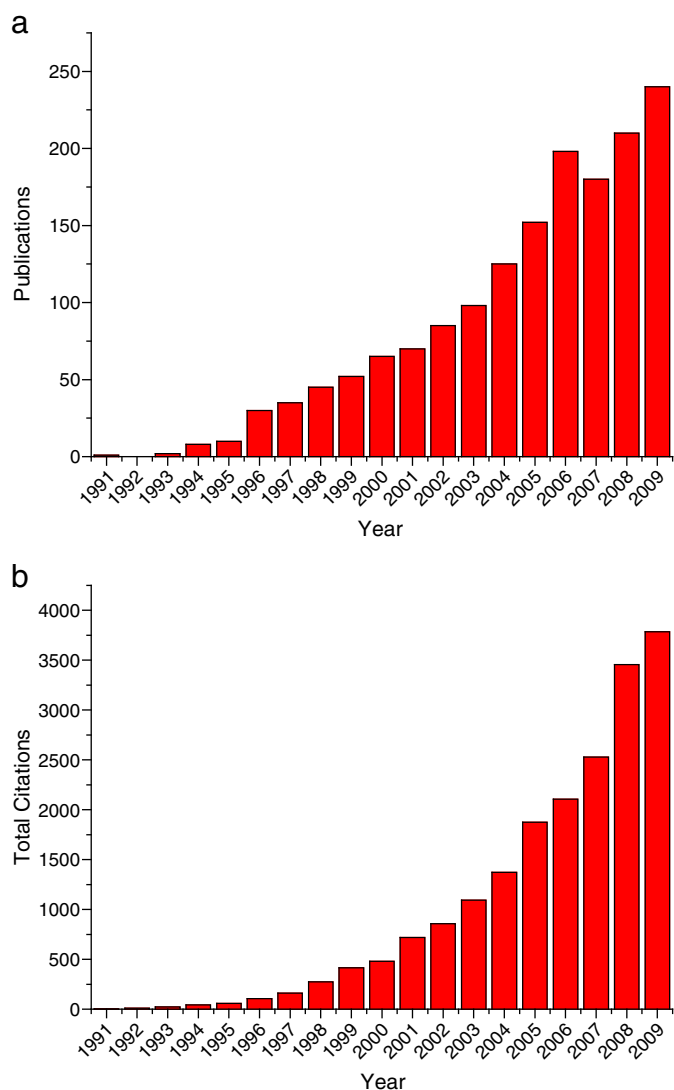


Fig. 1. (a). Total number of publications with topic "nanocrystalline diamond". (b). Total number of citations of publications with topic "nanocrystalline diamond". Source: Web of Science, Thomson Reuters.

mond and similar titles given to the same family of materials. The reason for the interest in thin films of high quality diamond is principally, but not exclusively, cost. If one can exploit the majority of the extreme properties of diamond or simply those that are required for a specific application with a thin film, then the added expense and complexity of growing bulks diamond seems superfluous. The growth of diamond is still a relatively expensive CVD or HPHT process and any reduction of growth duration is a real cost saving measure. There are also many applications where bulk diamond is inappropriate, such as Micro Electromechanical Systems (MEMS), tribological coatings etc. Nanocrystalline diamond exhibits many of the superior properties of diamond; those it does not are due to crystal size limitations. Good examples of these are electron/hole mobility and thermal conductivity, both obviously being limited by grain boundary scattering of electrons/holes or phonons respectively [1,2]. Obviously, the whole concept of a semiconductor relies on the extended periodicity of the lattice generating band structure, and the interruption of this has profound effects on carrier mobility values. The same is very much true for phonons. There are also mechanical properties that are affected by the grain size of nano-structured diamond and these will be detailed in later chapters.

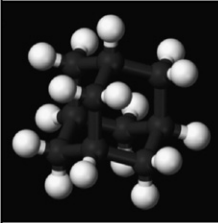
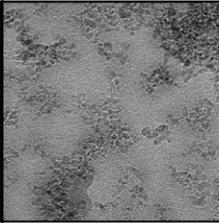
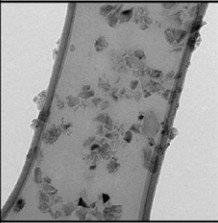
Nano-diamond particles have been used as abrasive materials for some time and have recently found more sophisticated applications such as single photon sources and bio-markers [3,4]. They are also of critical importance as seeds for the deposition of nano-diamond films [5]. One of the critical problems with such materials is the tendency of the core particles to aggregate into larger agglomerates which are difficult to disperse. This is a particular problem with material grown by detonation synthesis, in which the particles are tightly bound by sp^2 bonding formed during the detonation shockwave [6]. Thus, the purification of nano-diamond particles is an active and complex research area which will determine the applications of such particles [7–9].

2. Surface to volume ratio

At what size does tetrahedral bonded carbon cease to be diamond? The question may seem somewhat absurd given that the definition of diamond is the tetrahedral bonded allotrope of carbon. Perhaps a better question is at what size does tetrahedral carbon cease to behave like bulk diamond? Even "like" is probably inappropriate, for example, tetrahedral amorphous carbon (TaC), one of the Diamond-Like-Carbon (DLC) families, has many properties similar to diamond but is hardly considered to be diamond. The reason for this is simply that though DLC materials may constitute a considerable amount of sp^3 bonding (in some cases over 90%), they are fundamentally amorphous. Thus, the difference between DLC and bulk diamond is clear, and a question of crystalline structure. However, problems occur in definition at the transition between these two materials. As length scales become very small there is a real ambiguity in what constitutes a crystal. One can invoke the allotrope argument for carbon and say that diamond is an extended phase of sp^3 carbon, but this still does not put an absolute number on the length of the extended phase. This fundamental question appears in two distinct cases of definition, in diamond particles and films.

First we will address the issue of diamond particles, as the simplest system where the most unambiguous data is available. Diamond particles are available in various sizes from below 1 nm (adamantane diamantine, pentamantane etc., though strictly diamondoids), through <10 nm (originating from detonation processes and more recently PLD), to >20 nm (many production processes, jet milling, mechanical grinding etc.). A comparison of these particles is shown in Table 1. The smallest known diamond structured particles are in fact not strictly speaking diamonds, but diamondoids [10]. These particles are generally isolated from petroleum, being a source of many problems in natural gas, gas condensates and light crude oil flow systems where they can act as

Table 1
Types of nano-diamond particles.

Diamondoids	Ultra-dispersed diamond (UDD)	Sub micron diamond grit
		
< 1nm	< 10 nm	> 20 nm
Purification of petroleum	Detonation synthesis	Mechanical size reduction of bulk diamond

flocculation sources, blocking flow paths. A single adamantane molecule weighs 10^{-21} ct, i.e. 2×10^{-22} g. Adamantane is not truly a diamond as every carbon atom is at the surface and thus is bonded to at least one hydrogen atom. To date there are few applications of adamantane and the higher diamondoids and as they are not true diamonds they will not be discussed in detail here.

The next biggest diamond particle, and thus the smallest true diamonds, are made from detonation synthesis such as with trinitrotoluene (TNT) and hexogen [6]. During the detonation shockwave, the pressure and temperature reach the stability region of diamond in the phase diagram [11]. Thus, for a brief moment of typically around 1 μ s, diamond particles can be grown. These particles are usually called Ultra-Dispersed Diamond (UDD) and their mean size is quoted as around 4 nm [12]. This size results in a specific surface greater than 400 m²/g with more than 15% of UDD particle carbon atoms located at the surface [13]. This has profound implications on the surface chemistry and stability of such particles. It has been shown that diamond is actually energetically favoured over polycyclic aromatics for diameters of less than 3 nm with hydrogen termination [14]. Thus, at this length scale diamond cannot truly be said to be meta-stable. The reactivity of such fine particles can also differ substantially from bulk diamond surfaces [7].

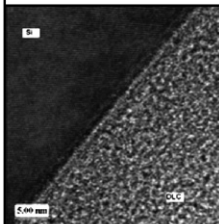
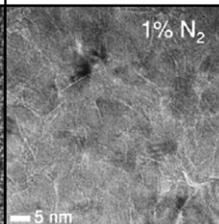
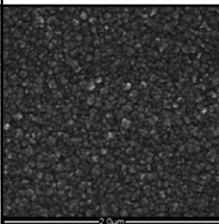
Finally, as one gets to sizes of greater than 20 nm, nano-diamond particles behave like bulk diamond. This is predominantly due to the far reduced concentration of atoms at the surface with regards to the bulk. These diamonds are usually produced from top down methods such as jet milling or abrasion of larger diamonds [15], an expensive and relatively time consuming process. However, their quality generally exceeds that of smaller diamonds due to their reduced surface to volume fraction. Their Raman and X-Ray diffraction spectra are far more reminiscent of bulk diamond than these smaller counterparts.

For films the difference is very much complicated by a terminology which is mostly historical. Nanocrystalline diamond was a term initially given to thin film diamond of poor quality. In the earlier days of diamond growth, when CVD reactor design was in its infancy and nucleation densities were very low, nanocrystalline diamond was a name given to thin diamond films which generally had low quality. Diamond growth evolved and high quality single crystal and microcrystalline films dominated research, leaving nanocrystalline diamond very much in the background. Recently, nanocrystalline diamond has developed into a sophisticated material with a wide variety of applications and terminology [16]. Table 2 attempts to clarify some of this terminology.

The smallest grain size diamond films are called ultrananocrystalline diamond (UNCD), a term originating from Argonne National Laboratory [17]. These films have grain sizes around 5 nm, with a considerable amount of amorphous grain boundaries which are very similar to Diamond-Like-Carbon (DLC). DLC is strictly speaking not diamond but is included in the table for clarity, and the fact the UNCD has many similarities with DLC. DLC has no crystalline structure as

Table 2

Types of nano-diamond films. UNCD TEM image reused with permission, copyright AIP 2001 [131], DLC image from K. Schirmer, J. Lutz: Deposition and characterization of amorphous hydrogenated diamond-like carbon films (a-C:H) Chemnitz University of Technology, Center for Microelectronics (ZfM), Annual Report 2004 http://www.zfm.tu-chemnitz.de/pdf/annual_report_2004/104-105.pdf. Used with permission.

Diamond-like carbon	Ultra-nanocrystalline diamond	Nanocrystalline diamond
		
Amorphous	< 10 nm	< 100 nm
No crystallinity, sp ³ content up to 30%	Re-nucleation results in no evolution of surface roughness	Little or no re-nucleation, films roughens with thickness

seen in the TEM image, whereas UNCD clearly exhibits the lattice planes of diamond, with amorphous DLC like regions between grains. UNCD is very much a special case, with all other types of nano-diamond films being termed nanocrystalline diamond (NCD). NCD films have grain sizes generally below 100 nm, but sometimes films with grains up to 500 nm are also labelled NCD [18]. Generally speaking NCD films contain less sp² and are thus more transparent than UNCD films; this is particularly acute when the films are grown without re-nucleation, i.e. with low methane concentration and high power density.

Perhaps the most convincing definition between the various forms of diamond is in their resulting properties. In this way it is easy to distinguish between nano-carbons, as measurements such as Young's modulus, optical transparency, thermal conductivity etc., are objective real world properties that can be quantified and exploited in real world applications. Ultimately the real world application arena is the true measure of a useful material and relegates all ambiguity and argument about material classification to semantics.

3. Nucleation

Successful growth of single crystalline diamond over larger areas and on foreign substrates is almost completely limited to growth on single crystal iridium [19]. Thus, diamond growth on the majority of foreign substrates results in polycrystalline material. Furthermore, efficient growth of diamond requires some kind of nucleation enhancement step. For example, the growth of diamond on untreated silicon results in nucleation densities of around 10^4 – 10^5 cm⁻² [20,21]. This is due to a combination of factors such as the high surface energy of diamond relative to silicon (6 J/cm² to 1.5 J/cm² respectively [22]), the relatively low sticking coefficient of gaseous precursors and the competition of nondiamond phases. An exhaustive review of nucleation mechanisms of thin film growth is beyond the scope of this review, for a more exhaustive review and comprehensive references, the reader is referred to an early review by Robins [23]. Suffice to say that nondiamond substrates require some pre-treatment in order to enhance the nucleation densities to the point where very thin (<50 nm) coalesced films can be grown. Numerous approaches have been used to enhance this nucleation density ranging from substrate abrasion, the addition of carbide forming or containing interlayers, through bias enhanced nucleation, to the application of monolayers of nano-diamond particles on the surface for subsequent growth. Research on these varying techniques goes back over 30 years and for the sake of brevity, this review will focus on those techniques which are able to realise the

higher nucleation densities ($>10^{11} \text{ cm}^{-2}$) required for high quality nanocrystalline diamond growth.

A caveat must be stated when comparing nucleation methods by their quoted nucleation density. In the early days of diamond growth, nucleation density was calculated by simply counting the number of diamond nuclei in a given area and dividing by this area. This was adequate in these cases as densities below 10^{10} cm^{-2} are easily quantified. Unfortunately, as nucleation densities exceed 10^{11} cm^{-2} , it becomes impossible to resolve individual nucleation sites and thus quantify their true concentration. For example, literature claims of densities of 10^{12} cm^{-2} or higher should be viewed with caution; as such a density would require 10 nm particles with no space between them or 5 nm particles with 5 nm gaps. Either is highly improbable and certainly not resolvable by AFM techniques when the tip convolution is taken into consideration [5], so the real question is where these numbers come from. Often they are very inaccurate estimates derived from surface coverage approximations, making the assumption of small particles

being close-packed which is not realistic. Firstly, such small (5 nm) particles are hard to develop and secondly they are part of a distribution of particle sizes which significantly disrupts close-packing arrangements as can be seen in Fig. 2(d). The nucleation density is quoted in the below technical descriptions, but the reader is warned of the questionable accuracy and suitability of such a number when assessing the quality of diamond nucleation treatments. Perhaps the real measure of the quality of a nucleation treatment is in the resulting diamond film, qualified by such objective measurements as its surface roughness etc.

3.1. Mechanical abrasion techniques (scratching)

The enhancement in diamond nucleation density of several orders of magnitude by scratching the substrate with diamond powder has been known for over 30 years [21]. In fact, a small enhancement has been observed even with nondiamond particles, but it is far less efficient than with diamond particles [24–26]. It is also common knowledge that the

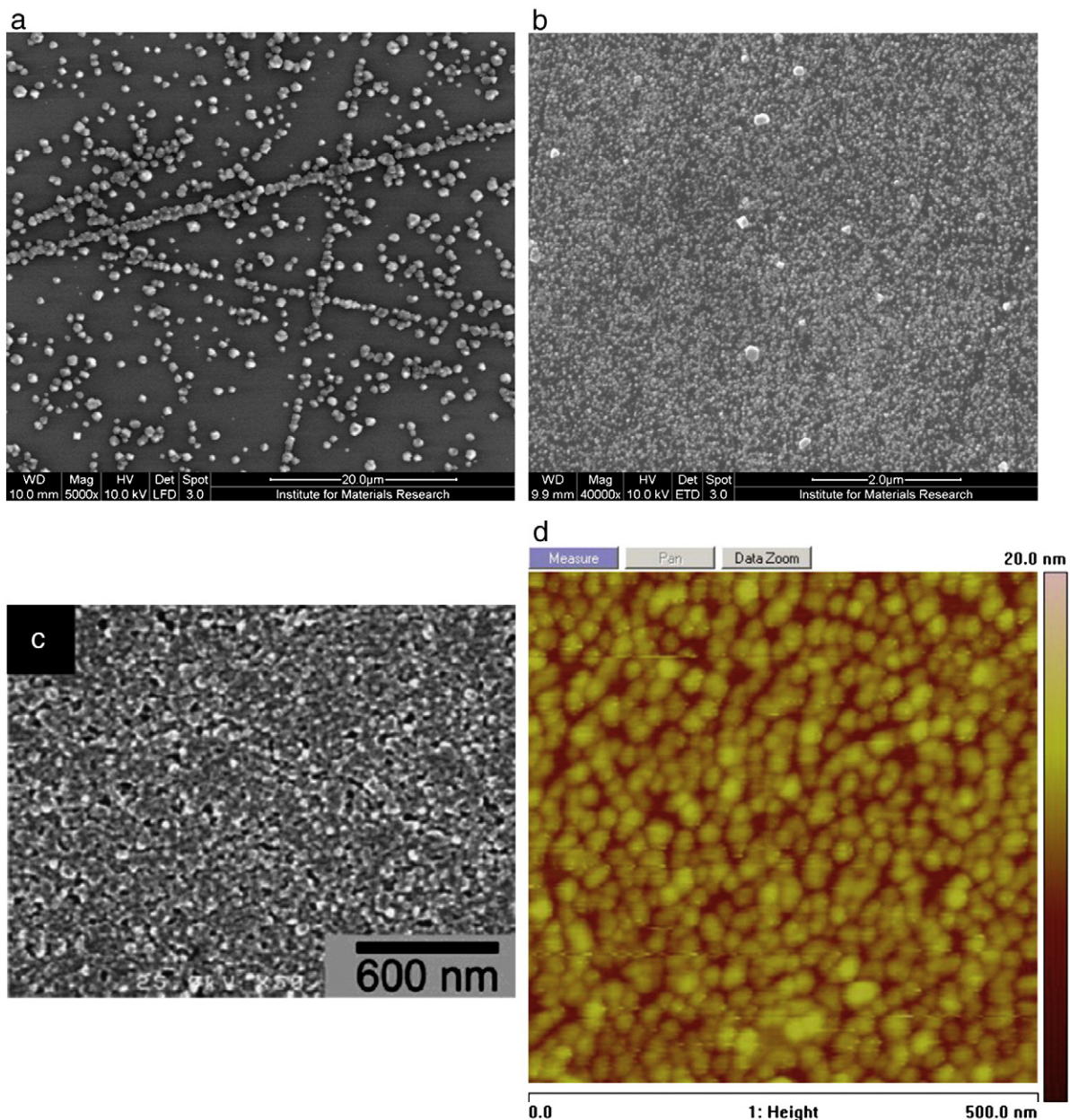


Fig. 2. (a). SEM image of mechanically scratched quartz after short growth duration. (b). SEM image of optimised mechanical seeding. (c). SEM image after short bias enhanced nucleation step. (d). AFM image of silicon coated with diamond nano-particles.

spontaneous nucleation of diamond crystals is mostly observed on defects on these mechanically damaged wafers, such as in scratches, pits, on grain boundaries etc. [25,27]. These features provide a large surface to volume fraction, leading to enhanced carbon super-saturation as well as a lower total free energy of the diamond nucleus due to reduced contact with the substrate surface. They also increase the amount of dangling bonds available for chemisorption and minimise steric hindrance. However, the principal mechanism behind the nucleation enhancement is the embedding of small residual diamond particles in the substrate, hence the process is far more efficient when utilising diamond particles in the polishing pad or cloth etc. Smaller diamond particles generally result in higher nucleation densities and better uniformity [28], presumably due to the larger surface to volume fraction of finer scratches and the increase of residual diamond. This technique realises nucleation densities up to around 10^{10} cm^{-2} , with the disadvantage of significant damage to the substrate from the abrasion process and the inability to treat three dimensional surface structures [29]. This can preclude its use for many nano-diamond applications, especially MEMS or optical coatings. Fig. 2(a) shows an example of poorly optimised mechanical seeding. It clearly shows the preference of diamond growth to grooves formed during the polishing. Fig. 2(b) shows an optimised mechanical seeding result, but there is still contamination of the surface with larger diamond particles. This leads to a kind of bi-modal distribution in the grain size, the small grains originating from diamond chipped into the substrate and surface damage as mentioned above, and the large grains coming from growth on the few large particles that could not be removed after scratching.

3.2. Ultrasonic particle treatment (micro-chipping)

Ultrasonic treatment of substrates in diamond slurries has been shown to enhance nucleation densities to 10^{10} cm^{-2} [28] and in extreme cases to 10^{11} cm^{-2} [30]. The mechanism of formation is very similar to that of mechanical abrasion, with the advantage of better uniformity and reduced polishing artefacts. By immersing a substrate into a slurry of micron sized diamond particles, the cavitations of the ultrasound cause similar damage to the substrate as with abrasion processes and also embed diamond fragments. HRTEM investigations have shown that the predominant nucleation mechanism is homoepitaxial growth on residual diamond embedded into the substrate [30], i.e. almost identical to the mechanical abrasion techniques. Contrary to abrasion techniques, the nucleation density actually increases with particle size, presumably due to very small diamond particles having insufficient momentum to damage the substrate or embed diamond fragments [28]. The lack of momentum has been improved by a synergistic approach using two particle sizes, fine diamond particles ($<0.25 \mu\text{m}$) with larger ($>2 \mu\text{m}$) diamond or nondiamond particles used to drive the smaller particles into the substrate, a so-called “hammering” approach [31]. This approach increases the nucleation density to amongst the highest reported for mechanical processes ($\sim 5 \times 10^{10} \text{ cm}^{-2}$) [31]. Variations on these substrate treatments in ultrasound with diamond slurries constitute the majority of what is used to nucleate diamond films today. They have the advantages of high nucleation densities, three dimensional substrate possibilities but with the downside of mechanical damage of the substrate. It is also almost impossible to remove all the larger sized diamond grit which leads to large disturbances in the substrate conformity, high local roughness etc. which are major problems for MEMS and tribological technologies where surface roughness must be as low as possible. This is shown in Fig. 2(b) which although is mechanically polished, is done so with larger grit and the effect of the large particles on the surface after a short duration of growth is clearly visible.

3.3. Carbon, carbide and carbide forming interlayers

Spontaneous diamond nucleation on substrates that form carbides has been shown to exceed that of those that do not by two orders of

magnitude [25]. DLC layers have been demonstrated to assist nucleation in the case of combustion flame synthesis [32], as have hydrocarbon oils, fingerprints and evaporated carbon in the case of hot filament assisted CVD (HFCVD) [33]. These carbon derived interlayers can assist nucleation processes in several ways. Firstly, it is likely that the sticking coefficient is higher on the carbide interlayer than the bare substrate, reducing the chance of re-evaporation of nuclei. Secondly, many substrate materials such as silicon have rather high carbon solubilities. Thus, carbon impinging on the substrate area where there is no nucleation site can diffuse into the substrate and be lost to the growth/nucleation process. This process will continue until the surface forms a carbide or the near surface is supersaturated with carbon, reducing the diffusion gradient [34]. This means that a high carbon content interlayer can act as a barrier to carbon in-diffusion into the substrate, resulting in a substantial increase in the availability of surface carbon. Thirdly, carbon growth species will have a low surface mobility on most substrates, whereas it is likely to increase on carbon saturated surfaces. Obviously, all these factors will increase the chance of critical nuclei being formed and increase their survival rate. Carbon, carbide or carbide forming interlayers have all been shown to locally increase the nucleation density. In fact, many substrates form carbides during the early stages of diamond growth [35,36]. Interlayers containing higher levels of sp^3 however, are known to have a more pronounced effect [37]. This is unsurprising considering their enhanced resistance to etching by atomic hydrogen over sp^2 bonding and the presence of sp^3 clusters which can become critical nuclei. Interlayers can enhance nucleation densities, but on their own are far less effective than the previously mentioned abrasion and ultrasound techniques which actually embed diamond nuclei into the substrates. Carbides will still form at the interface between the seeds and the carbide forming substrate, especially between diamond nuclei.

3.4. Bias enhanced nucleation

One of the few nucleation techniques that can be performed in-situ is bias enhanced nucleation (BEN) [38]. During BEN, the substrate, which must be conductive, is negatively biased by around 100–250 V DC with respect to the (grounded) chamber or a second internal electrode. This process is generally carried out under rather methane rich (4–10% in hydrogen) conditions as compared to diamond growth [39–41], and is most routinely used in microwave plasma enhanced CVD (MWPECVD) [39–41], although it may also be executed in HFCVD [42] and DC plasma CVD [26,43]. The mechanism behind BEN is generally accepted to be based on the sub-plantation model [44,45]. In this model, incident CH_4^+ ions have an energy distribution of around 80 eV, which is close to the optimum to sub-plant them into a-C [44]. This energy is also high enough to annihilate any surface nuclei and thus the possibility of surface nucleation is unlikely. There are two models for the nucleation sites evolving from this layer. In the first, it is argued that the high substrate temperatures promote the formation of nanocrystalline graphite, which can act as nucleation sites for subsequent diamond growth [44]. In the second, the nucleation sites originate from the formation of pure sp^3 carbon clusters in the layer, the annealing of faults under the presence of hydrogen and the growth of these clusters via the transformation of amorphous carbon into diamond. This sp^3 bonded layer forms a barrier to subsequent bombardment and results in the preferential displacement of further sp^2 bonds into sp^3 . On switching over to the regular CVD conditions, the remaining sp^2 is preferentially etched as the diamond grows. BEN can generally yield nucleation densities of around 10^{10} cm^{-2} having the advantage of being an in-situ process but with the disadvantage of the requirement of conductive substrates and difficulties in coating complex 3-dimensional shapes or large areas. Fig. 2(c) shows an example of very high nucleation densities achieved by Arnault et al., exceeding 10^{11} cm^{-2} [46]. Clearly in this case the surface is almost

completely covered and it is hard to assess the absolute nucleation density as the bias step is somewhat convoluted with growth.

3.5. Seeding with diamond nano-particles

One obvious approach to enhance diamond nucleation densities is to coat the substrate surface with as many diamond particles as possible, which act as the seeds for epitaxial growth. Proof of this epitaxial growth is clear from such work as Geis et al. who showed that (111) textured diamond films followed the seed texture [47]; this is probably the earliest example of seeding with diamond particles. This approach is obviously related to the above techniques involving particles but at a much lower length scale. In the early days of diamond growth, only the larger diamond particles were available (diamond grit), those shown in Table 1, from mechanical size reduction. These were somewhat larger than the smallest available today and thus were used microchip diamond fragments into the substrates (see Sections 3.1 and 3.2). The production of much smaller diamond particles by enhanced milling techniques and somewhat more significantly, detonation synthesis has resulted in new methods for the realisation of very high nucleation densities by substrate seeding [5,48]. These techniques have numerous advantages over the aforementioned methods, such as, no substrate damage, three dimensional possibilities and facile scale up. It should be noted that although these techniques are frequently executed with ultrasonic agitation, the basic mechanism of nucleation enhancement is electrostatic attraction of fine particles to the substrate. Thus, they are slightly complicated by colloidal chemistry and care must be taken with pH, concentration, zeta potential etc. to reach the highest nucleation densities [5,7]. The ultrasonic agitation helps to maintain the colloidal dispersion and improves the uniformity of the coating.

In the case of detonation nano-diamond particles, nucleation is complicated by the preparation of mono-disperse colloids of diamond nano-particles. During the detonation synthesis, significant sp^2 bonded carbon is also produced which leads to very tight agglomeration of the core diamond particles. These agglomerates can be over 100 nm so are obviously not useful in this form for high density nucleation. In order to break these agglomerates down into the fine 3–5 nm particles several techniques such as bead milling [8], burning in air [9], and hydrogenation [7,49] have been shown to be effective. The colloids resulting from these techniques contain particles with surface charges relating predominantly to their hydrogen or oxygen containing surface functional groups. Acid cleaned or oxygen/air burned particles have negative zeta potentials [9] and hydrogenated particles positive zeta potentials [7]. Thus, the zeta potential of the substrate must be considered for the nano-particles to stick efficiently, and both zeta potentials of the substrate and diamond nano-particles exhibit significant pH dependencies [7]. Several techniques have been shown to bypass this problem of surface charge such as the incorporation of the particles in a polymer matrix such as polyvinyl alcohol (PVA) [50] or sol-gel TiO_2 [51], however these approaches can also lead to aggregation of the nano-diamond particles. Another approach is to coat the substrate with a polymer of the opposite surface charge to the diamond nano-particles to enhance electrostatic attraction [52].

The key limiting parameter on the maximum realisable nucleation density is clearly the particle size distribution of the diamond nano-particle seeds. Obviously, the smaller the diamond particle can be made, the higher the nucleation density, provided that they can be prevented from aggregating. One possibility is thus to use adamantane as the seeds for nucleation, having a size less than one tenth the diameter of the smallest detonation nano-diamond particles. However, adamantane and the higher diamondoids have relatively low melting points and sublime at significantly lower temperatures than that of even low temperature diamond growth. Thus in general they are inappropriate for diamond nucleation in most cases. However, Tsugawa et al. have demonstrated that it is possible to utilise adamantane at exceptionally

low growth temperatures (150 °C) [53], yielding nucleation densities around 10^{11} cm^{-2} . In other work Giraud et al. covalently attached 2,2-divinyladamantane molecules to the {111} silicon substrate [54–56]. Unfortunately this only yielded nucleation densities of 10^8 cm^{-2} presumably due to the high temperature and low methane concentration used for the growth. It seems that the utilisation of adamantane for nucleation sites is complex and requires more study on the early stages of growth, in particular the stability of the seeds under atomic hydrogen flux. Unfortunately this technique has yet to demonstrate a significant improvement over optimised UDD nano-particle seeding, an example of which is shown in Fig. 2(d). It is clear from this image that the silicon surface is almost completely covered with close packed nano-diamond particles, yielding a nucleation density greater than 10^{11} cm^{-2} . It should be noticed that despite the high nucleation density the area of particle coverage is still rather low.

3.6. Combinatorial approaches

It is obvious that some of the aforementioned techniques could be combined to try and exploit synergistic effects such as those mentioned with the two diamond particle size “hammering approach”. Obviously, due to the carbon rich nature of the nucleation process, any mechanism which enhances the surface carbon concentration or provides a carbon diffusion barrier should be beneficial. It has been shown that thin layers of tungsten can enhance nucleation densities presumably due to the carbide formed at the interface blocking carbon diffusion into the substrate [57]. Similar approaches with other carbide forming materials could be expected to yield similar results [35,36]. However, metal inter-layers are certainly undesirable for optical coatings [29], and would also significantly spoil the Q-factors of MEMS devices.

Another novel combination of nucleation enhancement strategies was pioneered by Rotter et al. [58]. In this approach, the substrates are first coated with a thin layer of hydrogenated amorphous carbon (~10 nm) under normal CVD conditions, which will also form a carbide if the substrate is carbide forming [59]. Almost no diamond grows under these conditions due to the lack of nucleation sites. The substrate is then immersed into a slurry of diamond particles in an ultrasonic bath, and treated in much the same way as detailed in Section 3.2. This results in diamond fragments being embedded into the carbon layer and on subsequent growth, the carbon layer becomes a high concentration source of carbon for the particle growth and is completely removed during the early stages of growth [58]. In another variant of the approach one can seed on top of this carbon layer with nano-diamond particles as detailed in Section 3.5. Both approaches yield very high nucleation densities ($>10^{11} \text{ cm}^{-2}$).

Both of the above techniques provide enhanced carbon concentration during the initial stages of growth which results in significantly reduced etching of the diamond seeds and the underlying substrate. Another approach is to actually protect the diamond seeds with an over-layer. Lee et al. showed that a thin layer deposited over the nucleated substrate can increase the nucleation density by almost two orders of magnitude [60]. The effect of 50 nm thick Si over-layer is shown in Fig. 3, where the nucleation density is clearly much higher on the right side of the SEM image where the Si layer is. This layer acts as a protective barrier for the small diamond particles until they are large enough to resist the atomic hydrogen etching.

4. Growth and morphology

4.1. Incubation period

Due to the relatively short nature of nanocrystalline diamond growth runs and their thin film nature, the nucleation and early stages of growth are absolutely critical in the production of high quality material with low surface roughness and pin-hole density. The

nucleation stage has been described in detail above but it should be observed that it is very much convoluted with the early stages of growth. At the very beginning of a deposition run, there is a duration within which little diamond growth occurs, termed the incubation period. This is due to the incomplete coverage of the substrate with diamond nuclei, and carbon will diffuse into the substrate until either a carbon/carbide diffusion barrier is formed or the diamond nuclei have grown laterally enough to block this in-diffusion. At this point the film thickness will evolve at a significantly faster rate and the incubation period is over.

In conventional microcrystalline diamond growth the incubation period is not particularly significant as the films are too thick for the first few hundred nanometres of growth to be important. Free standing microcrystalline diamond plates also are often polished on both sides to remove this material. However, in the case of nanocrystalline diamond the first few tens of nanometres of the film are often a significant part of the film and certainly have profound implications on the surface roughness. For example, the nano-diamond seeds are etched during these early stages [20], which can lead to a reduction in nucleation density under low methane conditions. Thus it is generally beneficial to increase the methane concentration during the incubation period to reduce this etching [61]. The incubation period is also longer for substrates with high carbon diffusion rates, as obviously more carbon is lost from the nuclei growth into the substrate [22].

Fig. 4 shows the evolution of laser interferometer signal during the early stages of growth for various methane concentrations at high power density (3 kW microwave power at 60 mbar). Each curve represents the intensity of laser light reflected from the substrate as it is modulated by the constructive and destructive interference of light reflecting in the over growing layer. The first minimum of the curve represents 70 nm of growth and roughly half way between this point and the first maximum is the end of the incubation period at around 30 nm. Thus it can be clearly observed from these curves that the incubation period gets progressively shorter for higher methane concentrations. After 30 min the 0.5% CH₄ process has not even reached the end of the incubation period and thus there is likely to be significant etching at these power densities. The incubation period also depends on the power density in the case of MWPECVD and the substrate temperature in the case of all CVD methods [62]. Long incubation periods generally result in thicker SiC interfacial layers between the diamond and silicon substrate and thus, often films grown with higher methane concentrations exhibit less SiC, which on first consideration may seem counter-intuitive [22].

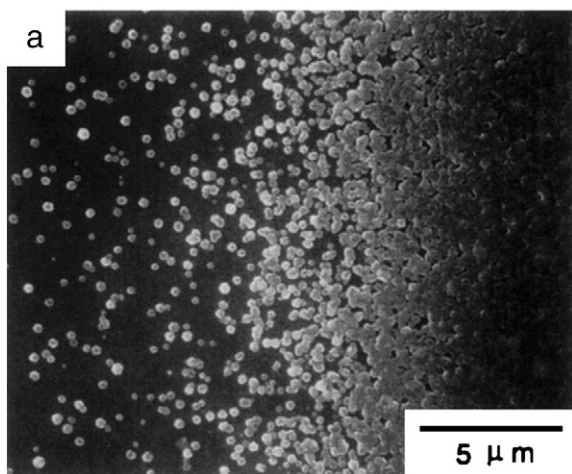


Fig. 3. SEM image of diamond abraded silicon with partial Si interlayer, Si coating is on the right of the figure.

Figure reused with permission from the Materials Research Society, copyright 1997 [60].

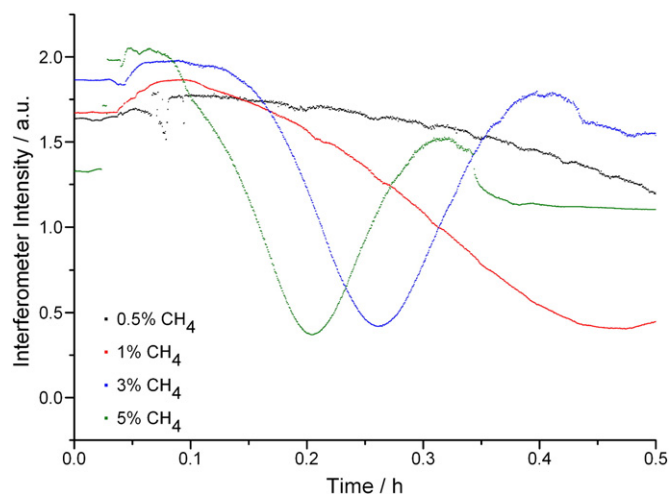


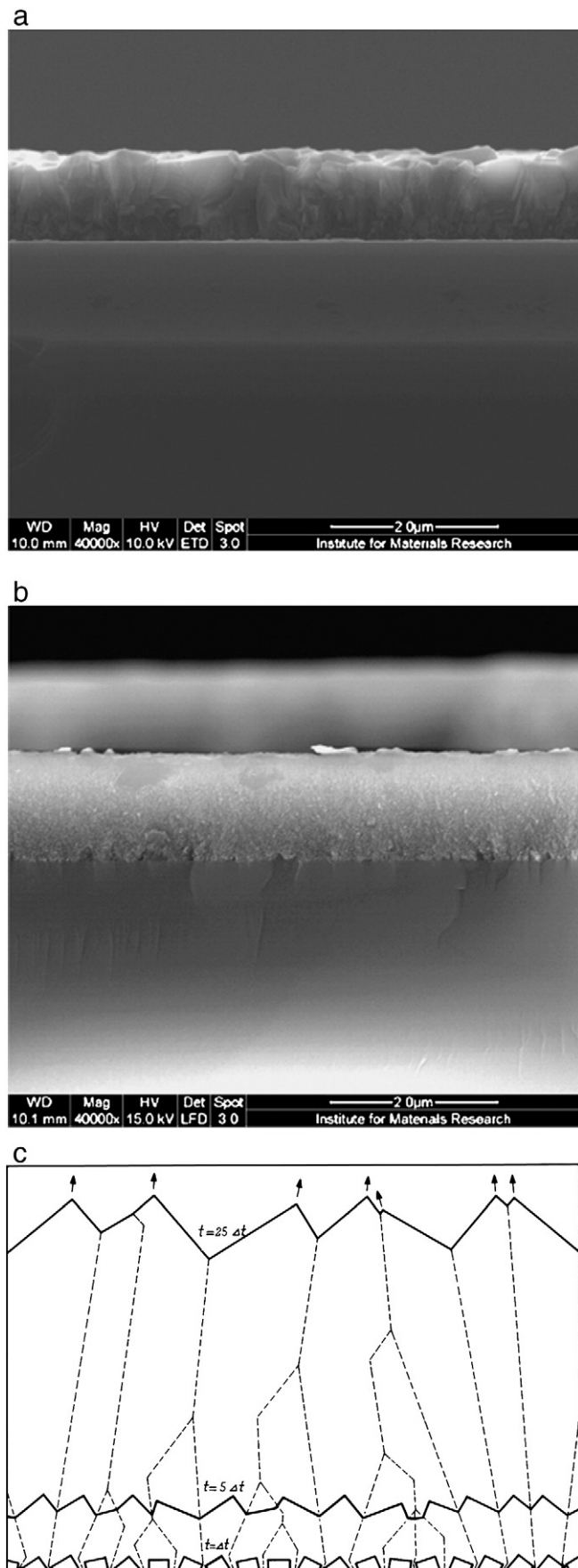
Fig. 4. Laser interferometry of the early stages of growth under various methane concentrations.

4.2. Suppression/enhancement of re-nucleation processes

Another regime in which nanocrystalline diamond growth differs from conventional microcrystalline growth is in the possibility of enhancing re-nucleation. Re-nucleation is the process by which the evolution of a crystallite is interrupted by secondary nuclei which triggers new, distinct crystallite growth. This has the effect of limiting the grain size and can be advantageous for the growth of films with reduced surface roughness, as is shown by the SEM cross sections in Fig. 5. The film in Fig. 5(a) is grown under low methane concentration, suppressing low nucleation processes. At one micron thickness it is already microcrystalline diamond due to the evolution of the crystallites, and clear columnar growth is evident. Fig. 5(b) is grown under Ar/CH₄ chemistry and thus enhanced re-nucleation processes. The film exhibits no visible crystallinity under this magnification and the surface roughness is independent of thickness. Fig. 5(c) shows the predicted evolution of crystallites from random oriented seed crystals. It can be seen that the columnar growth exhibited in Fig. 5(a) is what is expected in the absence of re-nucleation processes [63].

The advantages of re-nucleation come at a significant cost. Re-nucleation occurs because of the interruption of the layer by layer growth process by defects in the layer. This is obviously detrimental to the individual crystal properties and is more than likely sp² bonding or at least miss-oriented sp³ bonding. Thus, films grown with re-nucleation contain substantially more sp² bonding as characterised by Raman spectroscopy, more hydrogen and are generally black in appearance with a very high optical absorption coefficient [1,64–68]. Early nanocrystalline diamond films were mostly the result of high methane growth recipes under lower microwave power density conditions driving re-nucleation [69]. Other recipes followed such as the “hydrogen poor plasma” chemistry used by growers of ultra-nanocrystalline diamond (UNCD), which replaces the hydrogen of the growth process with argon, helium or nitrogen [70–72]. The results are very similar to increasing the methane concentration or reducing the microwave power density in conventional hydrogen plasmas [73]. This can be seen in Fig. 6 where the morphology transforms from no visible crystallinity under SEM to clear {100} faceting with reduction of the methane concentration during growth [74]. UNCD is very similar to the material shown in Fig. 6(a), and when grown under low nucleation density appears almost identical as is shown in Fig. 7. In fact, UNCD becomes progressively more crystalline with the addition of hydrogen into the gas phase, suggesting again that the re-nucleation process is suppressed by hydrogen [75].

Ultimately, most non-ideal diamond growth conditions will promote some kind of re-nucleation process be they high methane



concentrations, low power density, hydrogen replaced with noble gases, low pressure, continuous substrate bias etc. [74,76–78]. This has led many people to believe that nanocrystalline diamond is a low grade of diamond, and was often termed “cauliflower” or “Ballas type” diamond [74,79], and it is certainly true that all diamond types grown with enhanced re-nucleation processes have significantly higher sp^2 contents than those grown with the suppression of nucleation processes [73,80]. It should be noted that this does not mean all films grown with re-nucleation have the same sp^2 content; this is determined by the rate of re-nucleation. Some films grown with re-nucleation have grain sizes of the order of 30–50 nm which results in far less sp^2 than 3–5 nm films and can be highly transparent [64,81].

However, it is also possible to grow nanocrystalline diamond in the absence of significant re-nucleation processes, by using a very high initial nucleation density and short growth duration. Generally the methane concentrations used are far lower than that of re-nucleating processes [48,59,62,67,68,73,82,83]. This results in thin films of high quality diamond with nano-sized grains as the films are too thin for significant grain size expansion to have occurred [48,68]. In microcrystalline or single crystalline diamond growth, re-nucleation processes are suppressed as much as possible as larger grains lead to more bulk like diamond properties, such as high thermal conductivity, electron mobility, optical transparency etc. Nanocrystalline diamond films grown in a similar manner also exhibit many of these properties with the exception of those limited by crystallite size. Obvious examples are electron mobility and thermal conductivity both limited by grain boundary scattering processes be they electron/hole or phonon [1,2,65,84]. These films can be polished by Chemical Mechanical Polishing (CMP) processes to yield lower roughness than any as grown film, whether grown with re-nucleation or not.

4.3. Growth techniques

Nanocrystalline diamond films are readily grown by any of the conventional diamond CVD processes. These processes include Hot Filament CVD (HFCVD) [74,77,85], Direct Current Plasma CVD (DCCVD) [26,43,80,86,87], Microwave Plasma Enhanced CVD (MWPECVD) [48,62,68] etc. The basic requirement of all CVD diamond growth techniques is the generation of an abundance of atomic hydrogen [88]. The accepted model for CVD diamond growth has been exhaustively summarised by Butler et al. in the following reviews and the reader is referred to them [89–91]. Very briefly, during CVD the diamond lattice is stabilised by termination with atomic hydrogen. Atomic hydrogen produced by the activation technique (Hot Filament Dissociation, DC or Microwave Plasma) reacts with the source hydrocarbon creating a mixture of hydrocarbon species which include reactive carbon containing radicals. The atomic hydrogen also abstracts hydrogen from the CH surface, providing surface radical sites for carbon containing radicals to adsorb. However, much more frequently these are simply replaced with another hydrogen atom due to the relatively high concentration. It is this turnover of hydrogen atoms that also dehydrogenates the adsorbed carbon species and incorporates them into the lattice. Atomic hydrogen also reacts with sp and sp^2 carbon sites on the surface converting them to sp^3 carbon [91]. Thus, atomic hydrogen is critical for the CVD growth process and the efficiency of its production is a key parameter in CVD apparatus design. The hydrogen carbon growth species is generally accepted to be CH_3 [89–93].

It has been postulated that diamond can be grown in the absence of atomic hydrogen, with C_2 acting as a growth species rather than the more general consensus of CH_3 [70]. Early suggestions of this

Fig. 5. SEM cross sections of films grown with suppression (a) and enhancement (b) of re-nucleation processes, reused with permission, copyright Elsevier 2008 [68]. (c) Evolution of columnar growth from random-oriented crystals as predicted by van der Drift [63], copyright Philips 1967.

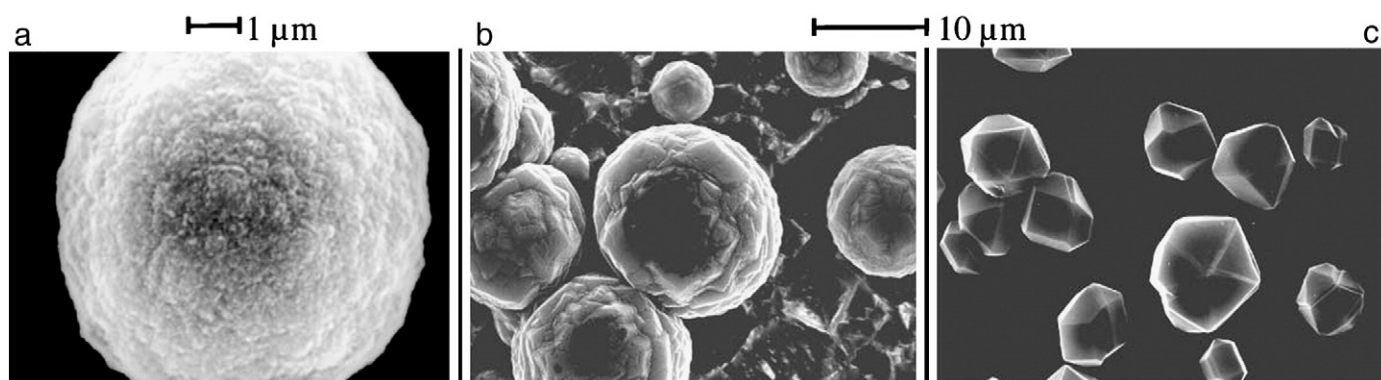


Fig. 6. Transition of diamond morphology from Ballas type to (100) facets. Reused with permission, copyright Elsevier 2002 [74].

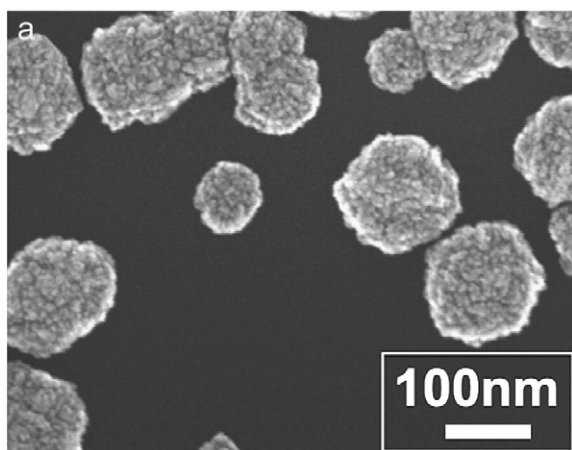


Fig. 7. SEM of early stages of UNCD growth. Reused with permission, copyright Elsevier 2006 [57].

originated from the observation of high C_2 intensity in the optical emission spectra (OES) of Ar/ CH_4 plasmas [94]. However, it is rather hard to make this claim from OES data alone, as the technique is not quantitative and other possible growth species such as CH_3 and C_2H_2 are not visible by emission. C_2 emission is also rather strong and is observed at high intensity in high power density/pressure conventional hydrogen plasmas. Later justifications were based on absorption spectroscopy, but the absolute densities were less than 10^{12} cm^{-3} [95], more than two orders of magnitude below the measured CH_3 concentration [89–93]. This was later confirmed by Cavity Ring Down Spectroscopy (CRDS), and specially resolved showing that the C_2 concentrations are significantly lower near the substrate [93]. Thus even though the sticking coefficient of C_2 is around an order of magnitude higher than that of CH_3 [96], the several

orders of magnitude lower concentration near the substrate suggest that it does not play a major role in nanocrystalline diamond growth [97].

Example conditions for nanocrystalline diamond growth by three techniques are listed in Table 3. This table is meant in no way to be exhaustive and the reader is referred to the references cited in the table and other sections of this review. Particular care must be made comparing growth conditions due to differences in reactor geometry which affect microwave power density in the case of MWPECVD and distances from filaments which affect radical concentrations in the case of HFCVD. For DC plasmas the field strength is rarely quoted, only the absolute voltage which is almost arbitrary. Filament temperature is often not quoted in the case of HFCVD and can be complicated to measure accurately. Temperature of deposition is always a large variable due to the multitude of methods to measure it and their associated errors. One general fact that can be taken from the table is that re-nucleation processes dominate under non-ideal conditions such as low power density or high methane concentrations.

Of particular importance for thin film growth is in-situ monitoring. Due to the thin nature of the films, it is important to have an accurate idea of the film thickness and growth rate during deposition. There are many ways to do this, but perhaps the most common is to use laser interferometry or monitor the interferometric effects of the film growth on the temperature as measured by optical pyrometry. An example of both these techniques is shown in Fig. 8. In this figure the temperature reading of the pyrometer (at 1.45–1.7 μm) is modulated by the interference from the growth of the film, the peak to valley distance represents around 165 nm. During the same growth, the thickness was also monitored by the interference modulation of the intensity of laser (633 nm) reflection. The peak to valley distance represents 75 nm in this case due to the shorter wavelength of the laser. Obviously shorter wavelengths and sharper grazing angle can increase the resolution further, but an improvement of greater than 50% would be difficult. The background signal from the laser

Table 3
Example conditions of nanocrystalline diamond growth.

	MWPECVD	HFCVD	DCCVD
Growth with re-nucleation	1% CH_4/Ar , 150 mbar, 1 kW, 800 °C [62,70] >5% CH_4/H_2 , 60 mbar, 3 kW, 800 °C [73]	2200 °C filament temp, >1.2% CH_4/H_2 , 15 mbar, 700 °C [77] 2% CH_4 , <40% H_2 , >50% Ar, 80 mbar, 870 °C [182]	9% CH_4/H_2 , 15 mbar, 500 V, 880 °C [181]
Growth without re-nucleation	>3% CH_4/H_2 , 15 mbar, 1500 W, 800 °C [73,74,116] 0.3% CH_4/H_2 , 15 mbar, 800 W, 720 °C [48] <3% CH_4/H_2 , 60 mbar, 3 kW, 800 °C [73] 0.5% CH_4/H_2 , 20–40 mbar, 600 W, 800 °C [46]	2% CH_4 , 49% H_2 , 49% Ar, 55 mbar [183] 2000 °C filament temp, 1% CH_4/H_2 , 70 mbar, 800 °C [31] 2% CH_4 , >60% H_2 , <40% Ar, 80 mbar, 950 °C [182] 1% CH_4 , H_2 , 30 mbar, 750 °C [184]	<2% CH_4/H_2 , >200 mbar, 4 A/cm ² , 850 °C [87]

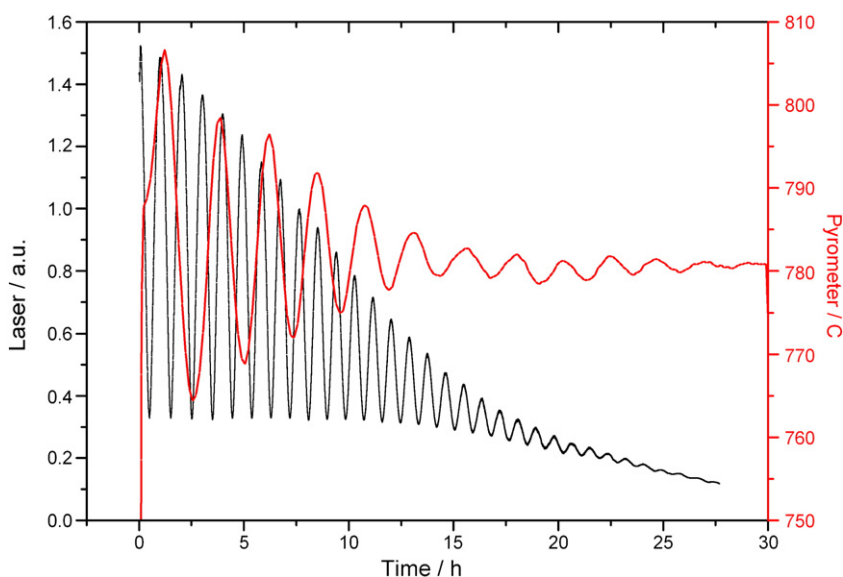


Fig. 8. Interferometry monitoring of laser reflectance and optical temperature measurements.

reflectance can be removed by lock-in techniques for further improvement in resolution [98]. For ultra high resolutions, in-situ spectroscopic ellipsometry can offer subnanometre performance [99]. Spectroscopic ellipsometry is a complex technique requiring sophisticated apparatus and modelling which is beyond the scope of this review; the reader is referred to the literature for details [99–102].

4.4. Grain size/surface to volume ratio, sp^2 and hydrogen content

The grain size of a nanocrystalline diamond film determines the surface to volume ratio, which is in turn the main determining factor in the sp^2 and hydrogen content. Obviously, smaller grains result in higher surface areas, which in turn lead to a higher sp^2 and hydrogen content due to the enhanced grain boundary volume [68,73,103–107]. Whilst it is true that not all grain boundaries are equal, all must contain some sp^2 bonding and hydrogen when grown by the CVD process and thus less grain boundaries will generally result in a higher overall percentage of sp^3 bonding. Fig. 9 shows how the grain sizes of 140 nm thick NCD films reduce with increasing methane concentration as re-nucleation processes become dominant [73]; this process happens at lower methane concentrations when the power density is lower as mentioned in previous sections. As the grains become smaller, the non-diamond content of the films rises drastically as is shown in Fig. 10 [73]. It can clearly be seen that at low methane levels the Raman spectra show clear evidence of diamond with a reasonably sharp peak at 1332 cm^{-1} ; obviously there is some peak broadening due to the low crystallite size and thickness of the film [108]. There is also some evidence of non-diamond carbon seen as a G-band at 1560 cm^{-1} arising from the in-plane stretching modes of sp^2 bonded carbon, presumably at the grain boundaries [109]. As the methane concentration is increased this band becomes more significant and eventually dominates the spectra. At the same time there is a significant broadening of the diamond peak by a twofold effect. First, there is enhanced broadening due to the reducing crystallite size with increasing methane. Second, the increased methane concentration leads to a higher concentration of disordered carbon, observed as the D-band, which is convoluted with the diamond peak [110,111]. The final feature of films grown with increased methane is the appearance of a peak at 1120 cm^{-1} which is always accompanied by a second feature at 1450 cm^{-1} . This pair of features has been ascribed to hydrogen/ sp^2 at grain boundaries [111–114]. In Fig. 10(b) it can be seen that the diamond peak is lost into the D-band very quickly, at around 3% methane. The G-band is already dominant at this methane level and a

significant contribution from hydrogen is present. The change in the Raman spectra is very much in tandem with the morphology. At very low methane contents there is little sp^2 due to a severely suppressed re-nucleation rate. As the higher methane concentrations and more significantly, lower power density regime drive the re-nucleation rate, the crystallite sizes decrease, increasing the surface to volume fraction of the films. The grain boundary concentration rises considerably, resulting in significantly enhanced sp^2 concentrations. This is clearly seen in the broadening of the diamond peak, its merging with the D-band and the eventual dominance of the G-band. Thus the increase of sp^2 bonding with reducing grain size is clear, and a similar thing is seen with hydrogen poor plasmas as shown in Fig. 11 [115]. It can be seen that the non-diamond carbon contributions from the aforementioned bands rise significantly with the Ar content/reducing hydrogen content of the plasma. Thus, the effect is rather similar to reducing the microwave power density or increasing the methane concentration. With no added hydrogen there is almost no evidence of diamond bonding as seen in Fig. 12(a) [68], where the diamond peak is completely convoluted with the D-band at this wavelength (632 nm). Fig. 12(b) shows an identical Raman spectrum from films grown with high methane concentrations in a conventional hydrogen plasma [116], confirming the earlier statements that there are several methods that lead to re-nucleation and they all result in increased sp^2 content in the films. Thus the term UNCD may not be of any real value when describing a subclass of NCD, far more specific would be “re-nucleating” or “non-re-nucleating” diamond when one wants to distinguish between the two classes of NCD.

Many NCD films are made up of grains that are too small to be accurately resolved by SEM and thus are best resolved by high resolution Transmission Electron Microscopy (TEM). An example of a TEM of UNCD is shown in Fig. 13(a) and (b) [115]. The sizes of the diamond grains are between 3 nm and 20 nm, the inset image of Fig. 13(a) is a selective area ($10\text{ }\mu\text{m}$ diameter) electron diffraction image showing only diamond features, obviously amorphous carbon would show no signature here. Fig. 13(b) shows that at higher magnification the crystals are between 10 nm and 20 nm in size and the lattice fringes of the {111} planes are evident (0.205 nm). Note that only the {111} planes are observable by TEM and only when properly oriented due to limits in resolution. TEM interpretation is rather complicated as only small areas of the sample are investigated due to the high resolution of the technique and thus the images cannot be truly claimed to be representative of larger areas. Fig. 13(a) and (b) shows evidence of some amorphous carbon as seen in the

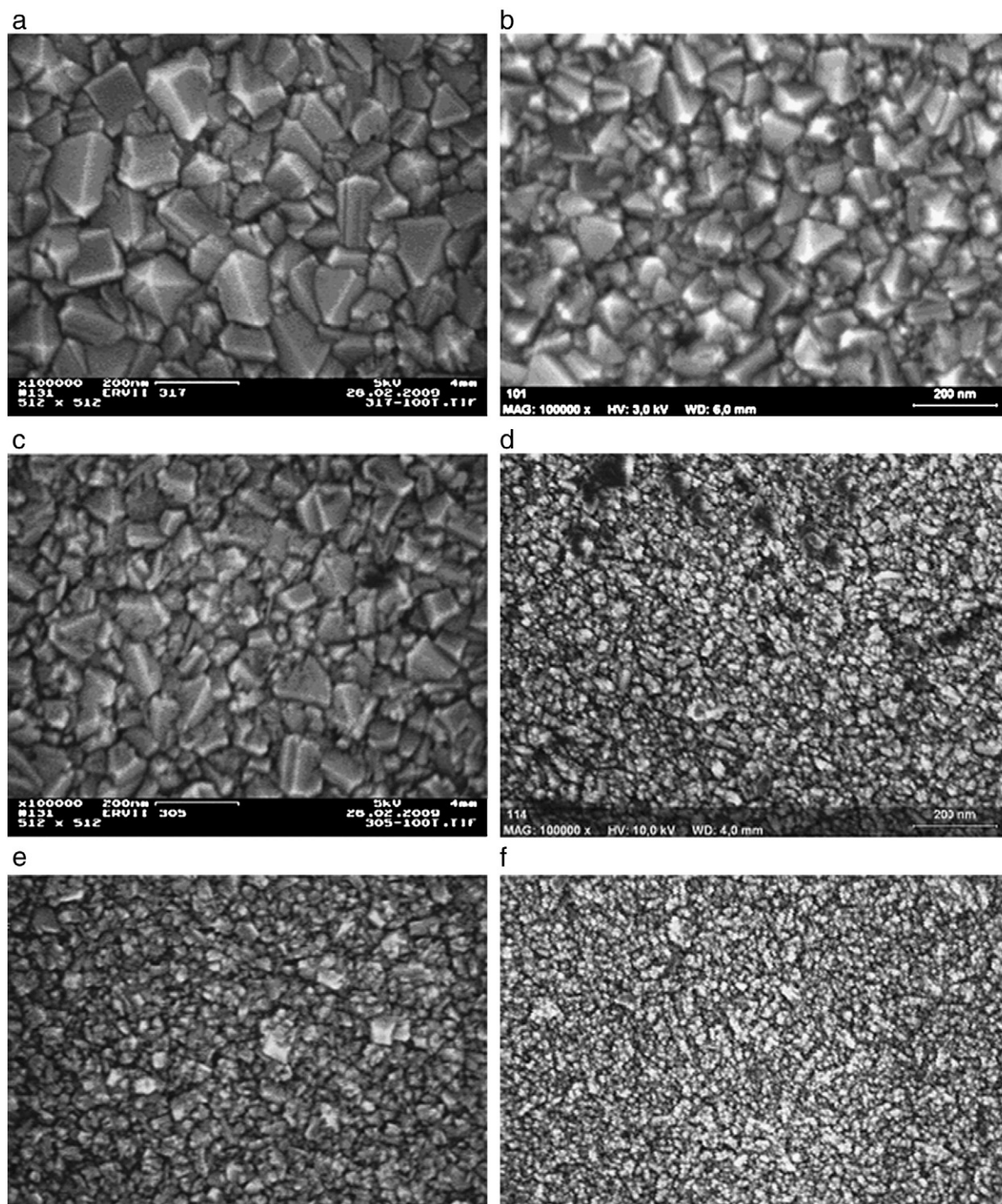


Fig. 9. SEM images of films deposited using two power density regimes (HPD = high power density, LPD = low power density). (a) 0.5% CH₄ HPD, (b) 0.5% CH₄ LPD, (c) 3% CH₄ HPD, (d) 3% CH₄ LPD, (e) 5% CH₄ HPD, and (f) 5% CH₄ LPD. Reused with permission, copyright Elsevier 2010 [73].

Raman spectra, with finite grain boundary volumes of noncrystalline carbon. The Electron Energy Loss Spectra of the same 10 μm diameter area is shown in Fig. 13(c). It is almost without any sp^2 signature (normally seen at 284 eV, π^*). The EELS spectra shows clear evidence of diamond σ^* bonding at 289 eV however.

Another technique for characterising the sp^2 content in diamond films is Near Edge X-Ray Absorption Fine Edge Structure (NEXAFS) [117,118]. The potential of NEXAFS for comparing carbon based films has been demonstrated by Capehart et al. [119], but particular care must be taken with carbon 1s edge absorption spectroscopy due to the

presence of carbon contamination on all monochromator optics. This adds structure to the spectra and is unavoidable. Fig. 14 shows the NEXAFS of diamond [111] and graphite [120]. Diamond exhibits a 1s absorption edge at 289.5 eV, a sharp bound exciton peak. There is some evidence of σ^* states at 302.5 eV just below the second bandgap. Graphite (HOPG) NEXAFS is dominated by the π^* antibonding state at 285.5 eV corresponding to out of plane bonds in the sp^2 bonding configuration [120]. More surface sensitive NEXAFS is able to see evidence of these on reconstructed diamond surfaces. The spectrum also exhibits features at 291 eV of a σ^* character and an exciton at

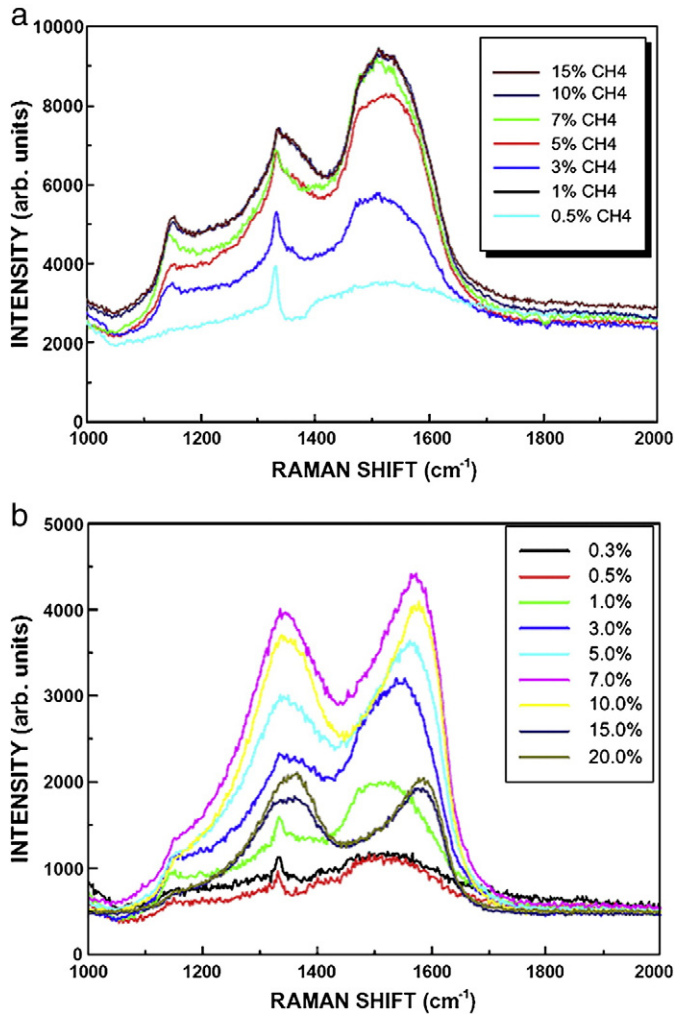


Fig. 10. Raman spectra of the two power density regimes (a) high power density, (b) low power density. Reused with permission, copyright Elsevier 2010 [73].

291.63 eV [120]. Obviously there is no evidence of a second bandgap. Fig. 15 compares the NEXAFS of (a) NCD grown with various CH₄ concentration and (b) NCD grown in Ar/CH₄ plasmas. It can be seen from this figure that the spectra are rather similar, that is NCD grown with high CH₄ resembles films grown with Ar/CH₄ plasmas, as seen before in the Raman spectra. Both show evidence of the diamond exciton peak, with the addition of some sp² features as detailed above. Thus NEXAFS correlates rather well with the Raman spectra and demonstrates again that UNCD films (films grown with Ar/CH₄ plasmas) are rather similar to NCD films grown with high CH₄ levels.

Hydrogen constitutes a relatively large concentration of nanocrystalline diamond films [105,107]. This is simply due to the fact that a small grain size results in a large surface to volume fraction where hydrogen can bond at the grain surfaces and in the non-diamond carbon at the grain boundaries. Fig. 16 shows the variation of hydrogen content in nanocrystalline diamond films as a function of grain size as determined by High Resolution Electron Energy Loss Spectroscopy (HREELS) [68]. It should be noted that there is some error in the grain sizes towards the lower end of the scale; error bars are omitted for clarity as the figure is not meant to be quantitative. Films at the lower end of the length scale contain substantially more hydrogen than films with larger crystals. This is not difficult to understand, as hydrogen content is expected to be much higher at grain boundaries and therefore it is ultimately a question of surface to volume fraction as mentioned above. As the grains get larger, the grain

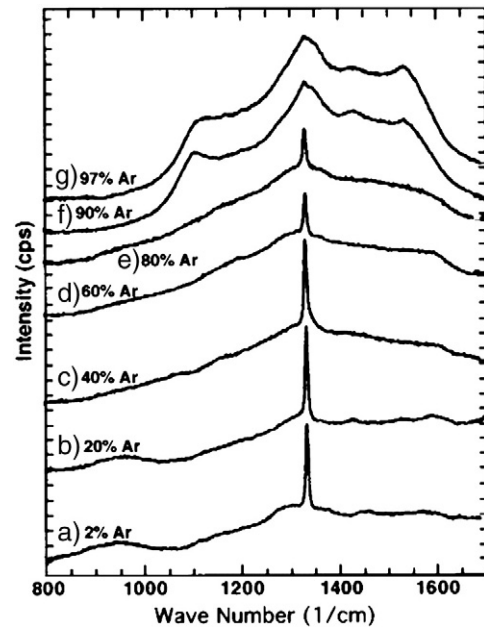


Fig. 11. Raman spectra of films deposited from Ar/H₂/CH₄ microwave plasmas with different reactant gases. Reused with permission, copyright AIP 1998 [115].

boundary fraction reduces considerably to the point where it is almost negligible, as in large grain size μ CD. Thus, the hydrogen content decreases substantially as the bulk of the hydrogen is located at grain

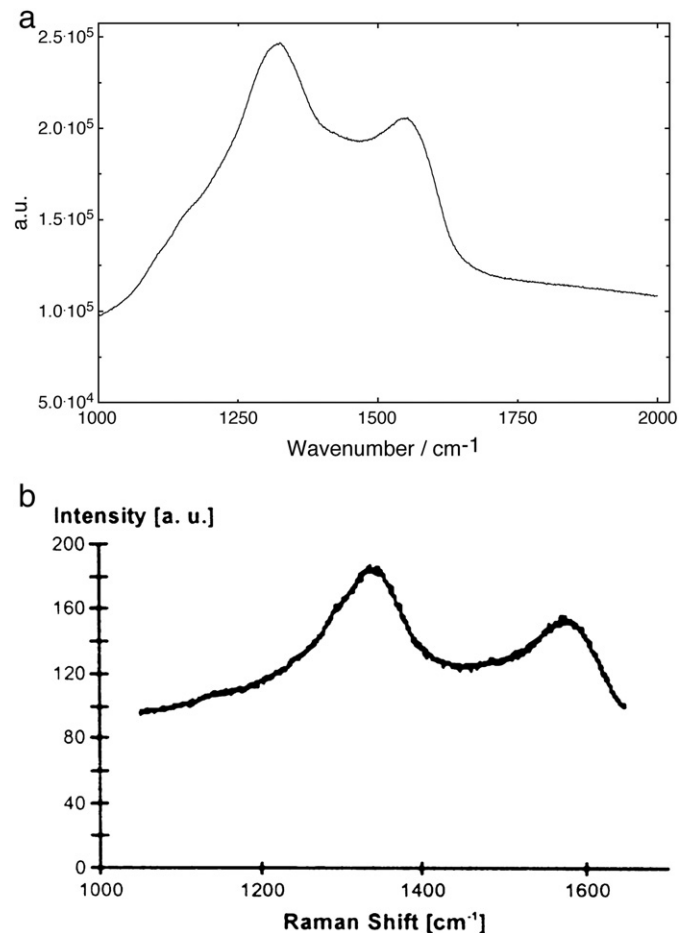


Fig. 12. Raman spectra of films grown (a) 1% CH₄ in Ar and (b) 10% CH₄ in H₂. Reused with permission, copyright Elsevier 2008 and 1999 [68,177].

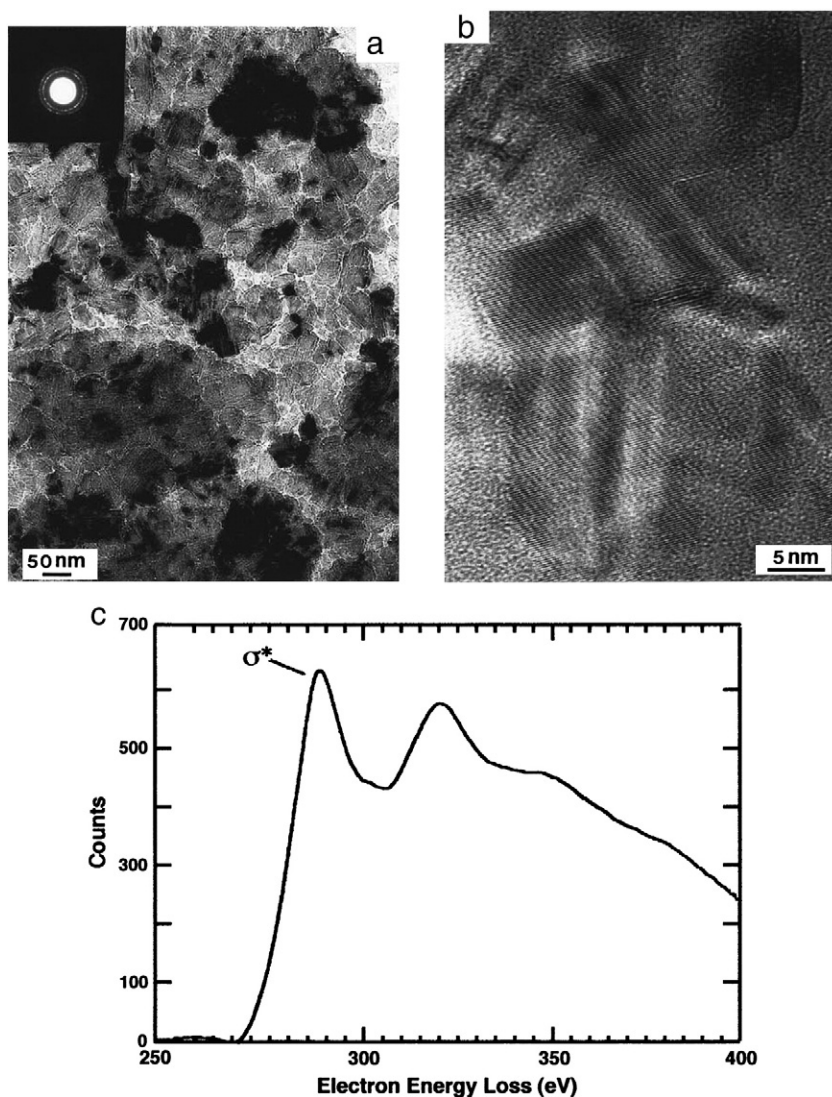


Fig. 13. (a) Low resolution TEM image of UNCD diamond film, (b) high resolution TEM image, and (c) EELS spectra of UNCD diamond film. Reused with permission, copyright AIP 1998 [115].

surfaces and in non-diamond bonding sites at the grain boundaries. A similar effect was observed with the previous Raman spectra at the 1120 cm^{-1} and 1450 cm^{-1} peaks, which become more prevalent at smaller grain sizes and are also due to hydrogen bonding.

4.5. Low temperature growth

Low temperature growth is obviously desirable for the integration of nanocrystalline diamond with silicon CMOS, or materials that melt at the conventional growth temperature of diamond. The growth of NCD at low temperature is no different to conventional diamond; the only real difference being the thicknesses required for application. With conventional microcrystalline diamond, low temperature growth becomes commercially unviable due to the low growth rates involved. This is far less of a constraint when submicron coatings are required. The activation energy of diamond growth on nondiamond substrates is an area of some ambiguity due to differences in deposition rate in nucleation and growth regimes, as mentioned above in the incubation period. Lee et al. have characterised these two regimes to be around 8 kcal/mol for bulk and 17 kcal/mol for nuclei in their reactor using real time in-situ spectral ellipsometry [99]. It should be noted that $8 \pm 3\text{ kcal/mol}$ {100} and $12 \pm 4\text{ kcal/mol}$ {111} have previously been reported for homoepitaxial growth and thus the

work of Lee et al. is in good agreement [121]. The values of activation energy reported in the literature vary widely due to differences in the incubation period, nucleation densities and the accuracy of temperature readings. For shorter growth durations such as those used with NCD the error is obviously significantly larger. Another key factor that is often ignored when quoting activation energies is the quality of the resulting NCD film. For example, one of the lowest values of activation quoted for NCD growth is $2\text{--}3\text{ kcal/mol}$ [122]. The quality of this diamond (grown from Ar/CH₄ process, re-nucleating UNCD) however, cannot be compared to films grown at similar temperatures with conventional H₂/CH₄ chemistry as shown in Fig. 17. In Fig. 17(a) the Raman spectra of films grown with the Ar/CH₄ process are shown as a function of temperature. The material shows a poor Raman spectra even at conventional temperatures, but at $400\text{ }^{\circ}\text{C}$ there is little evidence of diamond at 1332 cm^{-1} and strong signals at all sp² bands (1120 cm^{-1} , 1450 cm^{-1} and 1560 cm^{-1}), the spectra being dominated by the G-band and thus can hardly be claimed to be high quality faceted diamond. Fig. 17(b) shows a Raman spectrum of an example of NCD grown at $400\text{ }^{\circ}\text{C}$ with conventional H₂/CH₄ gas phase and hence suppressed re-nucleation. The activation energy of this growth process was nearer to 8 kcal/mol , i.e. higher than with the Ar/CH₄ process. The film exhibits clear unambiguous evidence for diamond at 1332 cm^{-1} with some evidence of a G-band. All other sp² signatures

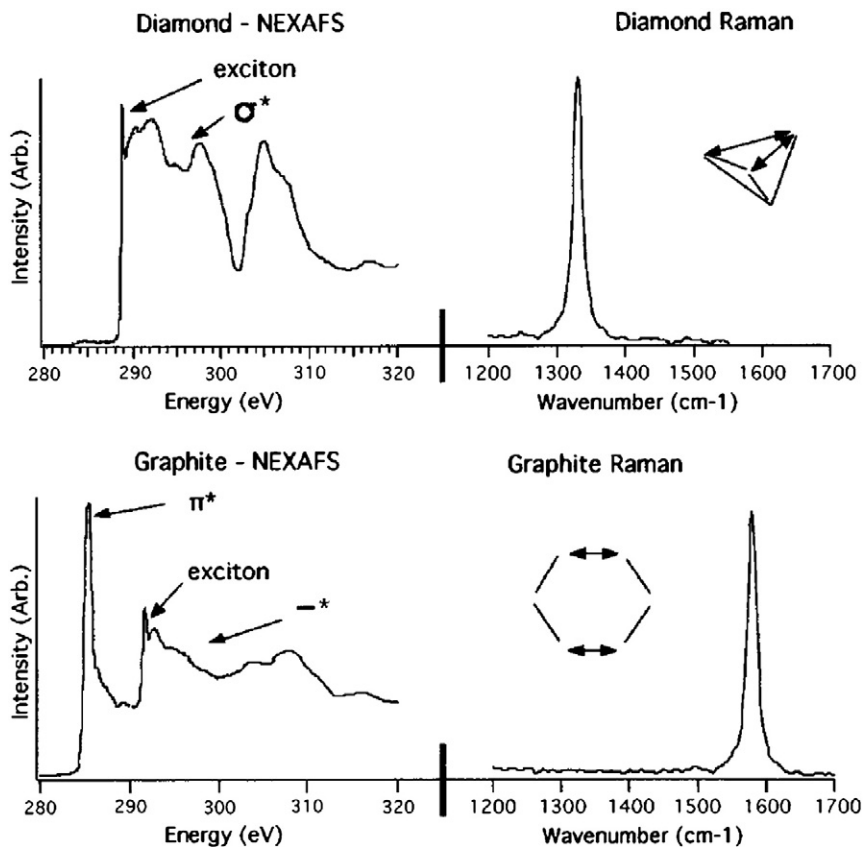


Fig. 14. NEXAFS of diamond {111} and graphite. Reused with permission, copyright AIP 1996 [120].

are suppressed due to the high quality faceting and low sp^2 content of this film. It should be noted that Fig. 17(a) was measured with a 633 nm laser whereas Fig. 17(b) with 458 nm. This will enhance the sp^2 signal somewhat in Fig. 17(a) but nowhere near enough to make the spectra comparable. Thus comparing activation energies is inappropriate as in the case of the Ar/CH₄ process, a significant

amount of the film is not diamond. The growth of diamond at such low temperatures has allowed the coating of CMOS electronics, glasses and plastics [29,123,124], and provides much promise for future applications of diamond. Perhaps the most convincing proof of the possibilities of diamond growth at low temperatures is the work by Tsugawa et al. [53]. In this work, diamond was grown below 150 °C

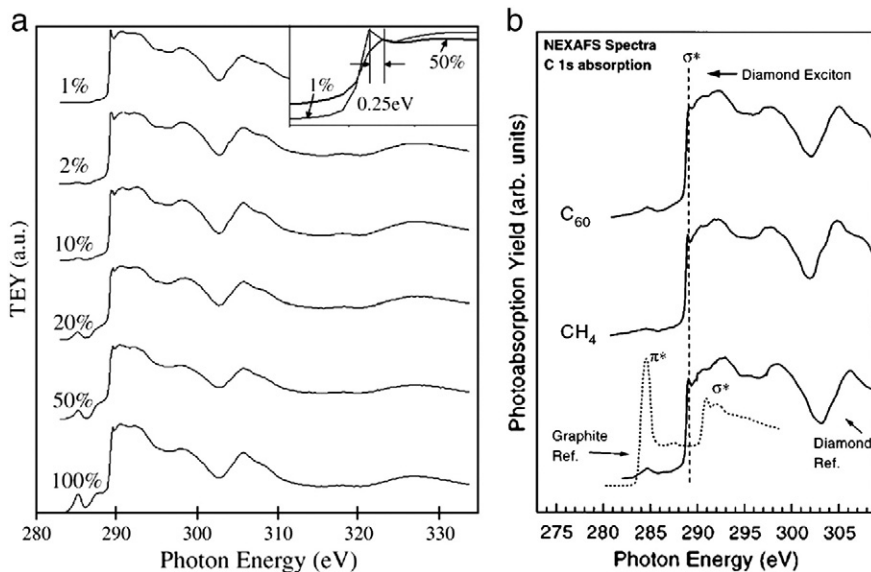


Fig. 15. NEXAFS of (a) NCD films grown with various CH₄ concentrations [178] and (b) NCD films grown in Ar/CH₄ plasmas [179]. Reused with permission, copyright Elsevier 2007 [178] and AIP 1996 [179].

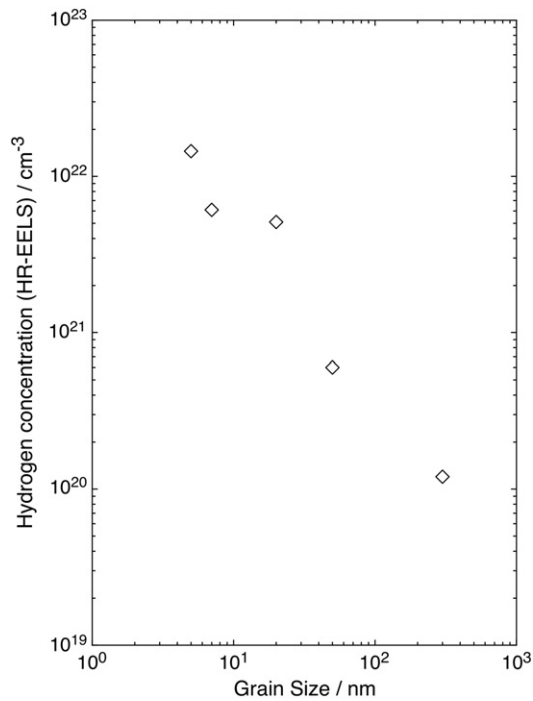


Fig. 16. Hydrogen content in NCD films as a function of approximate grain size as determined by HREELS. Reused with permission, copyright Elsevier 2008 [68].

which is confirmed by the fact that adamantane was used as nucleation sites, a molecule that sublimates at 250 °C. Thus although the adhesion and quality of diamond grown at such a low temperature are likely to be highly problematic, the growth of diamond at such temperatures is at least possible.

5. Thermal conductivity and Young's modulus

Thermal conductivity is a phonon scattering limited process in nanocrystalline materials and thus is strongly influenced by the grain size. This is clearly evident in Fig. 18. The thermal conductivity of films with very small (<10 nm) grain sizes is comparable to diamond like carbon and thus is of little use for heat spreading [125]. As the diamond grains approach 100 nm the thermal conductivity rapidly approaches that of bulk diamond [48]. Thus, thin films could be of use for heat spreading of active device areas. The Young's modulus of NCD films is also heavily dependant on the grain size and film quality. Fig. 19 shows how the Young's modulus of 140 nm thick diamond films decreases with increasing CH₄ concentration during growth and hence decreasing overall grain size [73]. The films characterised are the same as those in Fig. 9 and thus it is clear that again as the diamond grain size exceeds a few tens of nanometres, the films behave more like bulk diamond. These values of Young's modulus were derived from bulge tests and correlate well with values in the literature where small grain size UNCD type materials can have Young's modulus values as low as 440 GPa and films with greater than 50 nm grains exhibit Young's modulus values identical to single crystal diamond (1100 GPa) [73,82,103,126].

6. Optical and electronic properties

The optical and electrical properties of NCD films are a complex area with strong convolution between grain size and sp² bonding effects which has been summarised in a recent review [68]. The basic phenomena have been reviewed before in depth and the reader is referred to the following references for background reading upon which this section elaborates and brings up to date [1,2,64–

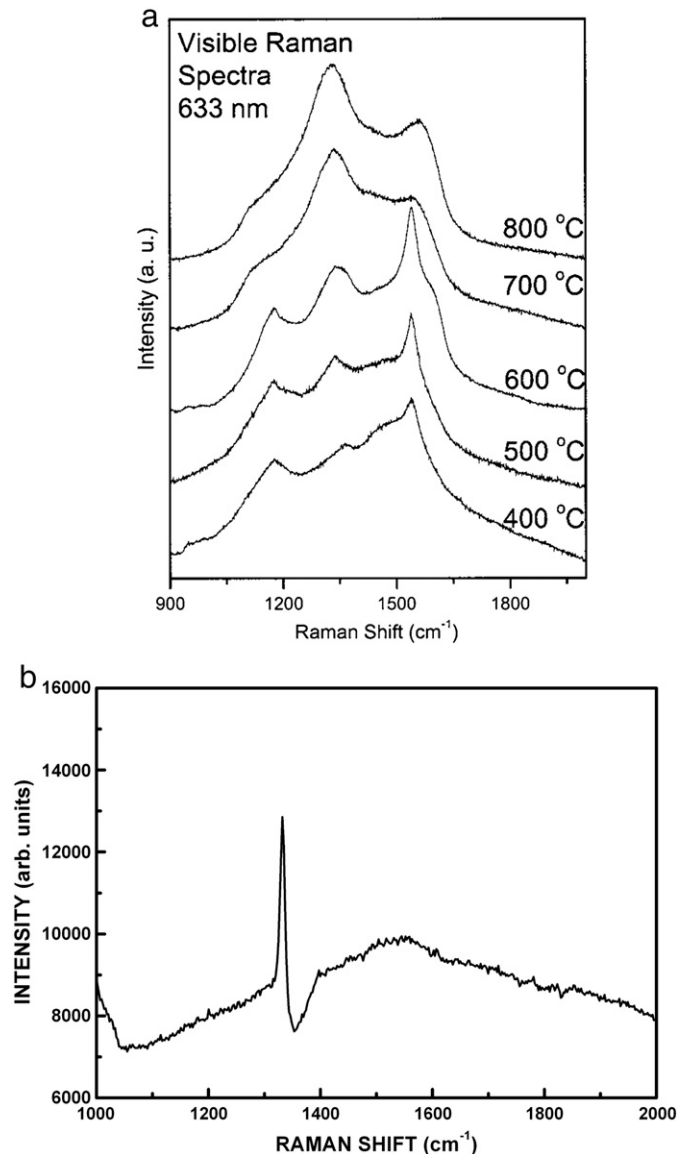


Fig. 17. Raman spectra of NCD films grown at 400 °C, 1% CH₄ (a) Ar/CH₄ process, reused with permission, copyright AIP 2004 [122], (b) H₂/CH₄ process.

68,84,100,127–133]. As demonstrated in earlier sections, the larger the grain size the closer the optical and electronic properties correlate with single crystal diamond. This is clearly seen in the optical transparency of the films. Re-nucleating diamond such as the aforementioned UNCD is black in appearance whereas NCD can have 80% transparency in the visible spectrum when a few hundred nanometres thick. This is shown more quantitatively in Fig. 20. Fig. 20 (a) shows the absorption coefficient of re-nucleating diamond types as measured by photo-thermal deflection spectroscopy (PDS) [64]. The spectra are clearly dominated by mid-gap absorption starting at around 0.8 eV which is attributed to transitions between π and π^* states [134]. The addition of nitrogen during growth (labelled here as 5%) broadens these bands substantially and saturates the PDS. The films labelled R contain grains around 3–5 nm whereas the grain size of sample AAu is nearer to 20 nm. Thus the slightly larger grain size shows a marked improvement in transparency. This is far clearer in Fig. 20(b) where the grain size is around 100 nm. Here the undoped material displays two orders of magnitude lower optical absorption coefficient compared to Fig. 20(a), though there is still some evidence of mid-gap absorption due to sp² bonding. The addition of boron results in substantially increased optical absorption coefficient but is

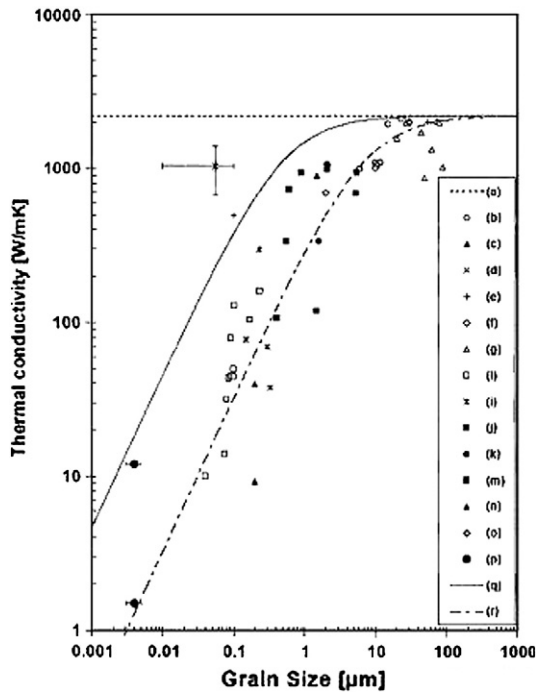


Fig. 18. Thermal conductivity vs grain size for NCD films. Reused with permission, copyright AIP 2006 [180].

still significantly below that of re-nucleating diamond grown with nitrogen. Thus the grain size is a critical determining factor in the optical transparency as small grain sizes result in a larger grain boundary volume and thus higher sp^2 content. Whilst it is true that some grain boundaries are wider and contain more sp^2 bonding than others, the general rule is that smaller grain sizes result in increased optical absorption due to enhanced grain boundary volume. This is shown schematically in Fig. 20(c), where the effects of band tailing and the appearance of π bands can be clearly seen introducing new optical transitions within the bandgap [134].

The smaller grain size materials grown with re-nucleation demonstrate unusual conductivity behaviour when compared to films grown without re-nucleation. This is shown in Fig. 21. Firstly, films with such small grain sizes and hence larger grain boundary volumes do not demonstrate very high resistivity, more than 3 orders of magnitude lower than NCD films. As previously shown in the Raman and optical absorption data this is due to the enhanced sp^2

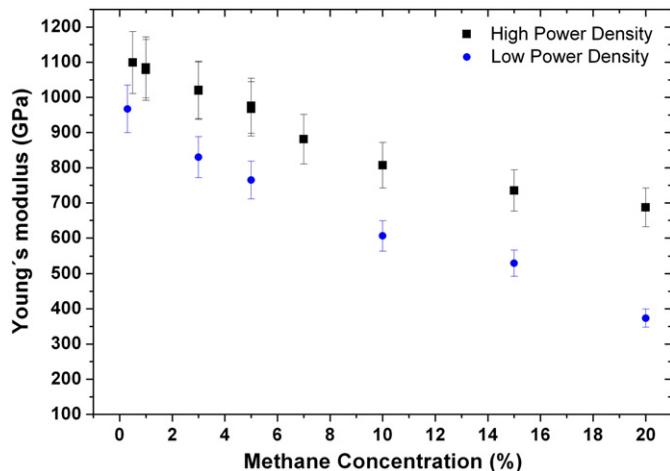


Fig. 19. Young's modulus as a function of CH_4 concentration during growth of NCD films. Reused with permission, copyright Elsevier 2010 [73].

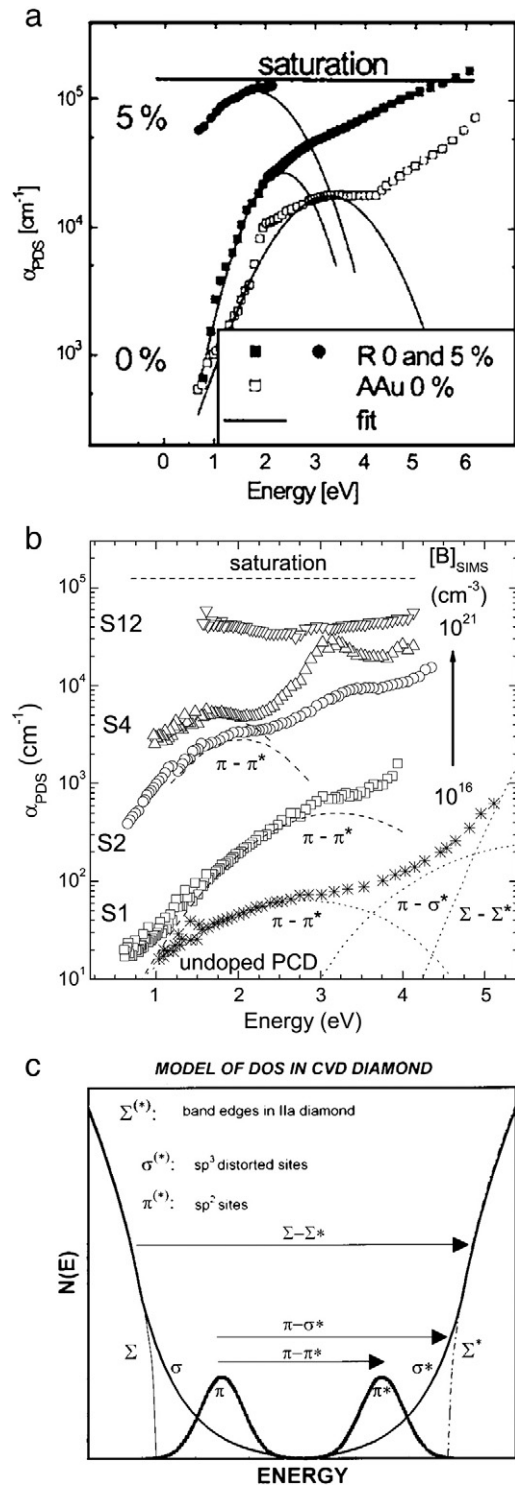


Fig. 20. Absorption coefficient measured by PDS for (a) re-nucleating diamond (UNCD, grain size <10 nm), reused with permission, copyright AIP 2006 [64] and (b) NCD grown without re-nucleation (grain size 100 nm) [2], reused with permission, copyright The American Physical Society 2009. (c) Schematic model of the density of states for NCD [134], reused with permission, copyright the American Physical Society 1996.

content of these films. The addition of nitrogen increases the conductivity sharply, but at high concentrations, far above conventional doping levels. At around 5% nitrogen addition, the films exhibit n-type conductivity which is metallic like in behaviour [84]. Measurements of the nitrogen content such as ERDA and SIMS show that there is little correlation between the nitrogen content in the

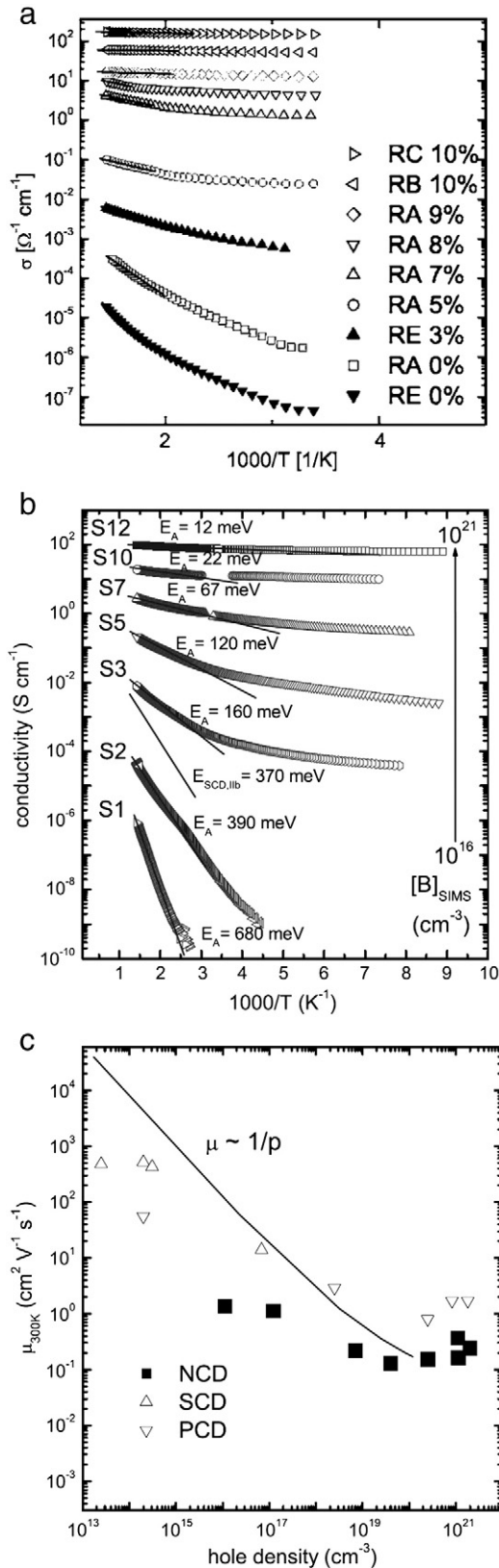


Fig. 21. Arrhenius plots of conductivity for (a) re-nucleating diamond with the addition of nitrogen [1], copyright The American Physical Society 2006, and (b) NCD grown without re-nucleation with the addition of boron [2], copyright The American Physical Society 2009. (c) Mobility of NCD vs carrier comparison compared with single crystal diamond (SCD) and polycrystalline ($>10 \mu\text{m}$ grain size) diamond (PCD) [2], copyright The American Physical Society 2009.

films and their conductivity [1,131]. The spin density as determined by ESR is also independent of nitrogen concentration, suggesting that the conductivity is only indirectly manipulated by nitrogen addition into the plasma [1]. This means that nitrogen itself is not a dopant and the conductivity behaviour is very similar to TaC films grown with nitrogen addition [135]. The increase in conductivity is explained by a broadening of the π and π^* bands which dominate the transport behaviour due to their lower energy levels around the Fermi level when compared to the σ and σ^* bands (see Fig. 20(c)). Thus although these films can show evidence of diamond band structure, albeit with a lower gap due to disorder, these states are dominated by the sp^2 states and thus the conductivity has little to do with diamond or doping [1,66].

The comparison with NCD films is stark as shown in Fig. 21(b). NCD films exhibit very high resistivities when undoped, approaching that of single crystal diamond ($>1 \times 10^{10} \Omega$). The addition of boron leads to p-type conductivity and the films behave identically to single crystal and microcrystalline diamond films albeit with a lower mobility and hence lower overall maximum conductivity [2]. The activation energy of the conductivity is comparable to that of single crystal and microcrystalline diamond films. Films with doping levels below 10^{19} cm^{-3} exhibit clear valence band activated transport, with hopping transport between 10^{19} cm^{-3} and $2 \times 10^{20} \text{ cm}^{-3}$ and finally metallic transport at higher doping levels [2]. These transitions correlate exactly with data in the literature on single crystal and microcrystalline boron doped diamond [2]. At metallic levels of doping the Raman spectra show Fano-interference between the continuum of electronic states introduced by the dopants and the zone-center phonon [2]. The films also exhibit superconductivity at low temperatures [2,127–130]. Both of these phenomena are beyond the scope of this review and the reader is referred to the aforementioned literature for further detail.

Thus the transport phenomena of NCD films with boron doping are easily explained by conventional doping of diamond by boron. Neither the smaller grain size material grown with nitrogen nor the boron doped NCD is able to realise high mobility values due to their small grain sizes, so neither is appropriate for active electronic device applications. This is clearly shown in Fig. 21(c) where the values of carrier mobility for NCD and UNCD are around $1 \text{ cm}^2 \text{V}^{-1} \text{s}^{-1}$ regardless of doping concentration [2,84]. Obviously single crystal diamond and large grain size polycrystalline diamond demonstrate a pronounced increase in hole mobility as the boron doping level is decreased.

Despite these low mobility values, both can be of use as high temperature stable (and in the case of NCD grown without re-nucleation, UV transparent) electrodes to materials such as SiC, GaN and in the case of re-nucleating diamond, even single crystal diamond [136–138].

7. Applications

Obviously, any application which can exploit the properties of diamond in a thin film configuration could profit from the integration of nanocrystalline diamond. This is especially apparent in passive applications such as heat spreading, tribology, optical coatings etc. [68]. For example, the high thermal conductivity of NCD films makes it of interest for Silicon on Diamond applications [102,139–142]. Coatings of NCD can have friction coefficients as low as single crystal diamond [143]. In such tribology applications, re-nucleation can be beneficial due to the absence of increasing roughness with thickness. For optical coatings it is more desirable to grow without re-nucleation for enhanced transparency [29,68].

More recent applications have surfaced due to the unique properties or configuration of NCD films. A particularly acute example is that of Micro or Nano Electro-Mechanical Systems (MEMS & NEMS). The fabrication of such structures with single crystalline diamond or microcrystalline diamond is highly problematic; one requires thin films of diamond on a sacrificial layer such as SiO_2 for most structures.

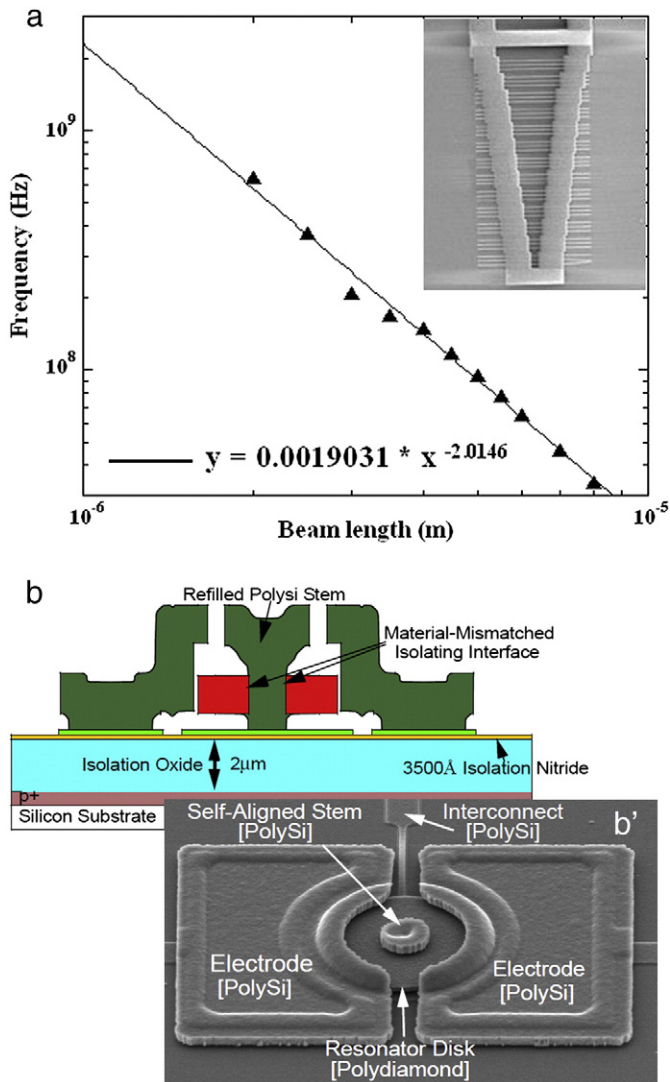


Fig. 22. MEMS structures from NCD. (a) Cantilevers and their resonant frequency as a function of beam length, reused with permission, copyright AIP 2002 [83] and (b) diamond/silicon disk resonator, figure re-used with permission [154], © 2004 IEEE.

With NCD films this is possible and allows the fabrication of a diverse array of micro and nanostructures [83,103,126,144–153]. Fig. 22 shows two examples of such structures. Fig. 22(a) shows double clamped cantilevers fabricated from a 180 nm thick NCD with a Young's modulus of around 840 GPa [83]. These cantilevers show resonant frequencies up to 640 MHz at 2 µm length, almost double the value for similar values fabricated from poly silicon [83]. The aforementioned work demonstrating Young's modulus values as high as 1100 GPa [73] could increase this frequency even further, though care must be taken when comparing different values of Young's modulus evaluated by different techniques [149]. It should be noted that fabrication with diamond is no more complex than poly silicon, in fact it can be easier due to the lack of the requirement of critical point drying due to the strength of diamond. Fig. 22(b) shows an example of a disk resonator where the silicon disk is replaced by diamond [154]. This device exploits the phonon mismatch between diamond and silicon, which is very high. As the disk is driven into oscillation, very little energy is lost by coupling into the stem due to the acoustic impedance differences between silicon and diamond. This results in very high Q values and this device broke the silicon record for frequency Q product when it was first demonstrated at 1.5 GHz [154]. The structure is complex, requiring multiple levels of lithography and demonstrates the possibility of integrating diamond with silicon technologies. Other complicated MEMS/NEMs structures have been

fabricated from NCD such as ring resonator arrays for RF signal processing [155], photonic crystal micro-cavities [156], whispering gallery mode micro-disks [157], to name but a few. Several piezo-electrics have been integrated with NCD such as langasite [158], gallium phosphate [159], PZT [160], ZnO [161,162], AlN [163] and quartz [164] as drivers for QCM, SAW and cantilever diamond structures [165].

NCD is not appropriate for active electronic device applications as mentioned above, however diamond is an outstanding electrochemical electrode [166]. As electrochemical reactions occur at the surface of diamond there is no need for large volumes of diamond bulk, thus high quality NCD surfaces can suffice [167]. Boron doped NCD can be grown on transparent substrates for use as a transparent electrochemical electrode [168–170]. This has numerous applications such as spectro-electrochemistry and transparent conductive electrodes for cell growth studies [171–175]. As a solid state electrode, NCD can also be used for field emission devices [176].

8. Conclusions

Nanocrystalline diamond is a diverse array of diamond materials best distinguished by the average grain size. This one feature determines almost all of the properties of the resulting film with larger grain sized material behaving more like bulk diamond and smaller grain size material more like DLC. Thus it is possible to be “too nano” for some applications, such as optical coatings for example where very small grain sizes necessarily increase the grain boundary volume fraction and hence the density of states within the bandgap due to sp^2 bonding. The consequence of small grain sizes is obvious when sp^2 bonding is considered. NCD is significantly different to amorphous silicon in this respect due to carbon allotropes. Small grain sizes increase the grain boundary volume fraction and the amount of nondiamond carbon, thus they will tend to make the film properties deviate from bulk diamond properties. Thus one must tune the properties of NCD films to their application, and most of this tuning involves controlling the grain size. It has also been suggested in this review that the definition of ultrananocrystalline diamond (UNCD), the moniker for films grown by the Ar/CH₄ process is not a helpful terminology. This is mostly down to the fact that similar films can be grown by other techniques and it makes more sense to differentiate films by their properties rather than by their growth process. The application field of NCD films is young and evolving from passive applications such as optical coatings, heat spreaders, tribology etc. to advanced MEMS devices and quantum optic devices. This future is exciting and time will tell where the future for this new form of diamond lies.

References

- [1] P. Achatz, O.A. Williams, P. Bruno, D.M. Gruen, J.A. Garrido, M. Stutzmann, *Physical Review B* 74 (15) (2006) 155429.
- [2] W. Gajewski, P. Achatz, O.A. Williams, K. Haenen, E. Bustarret, M. Stutzmann, J.A. Garrido, *Physical Review B* 79 (4) (2009) 45206.
- [3] J.R. Rabeau, A. Stacey, A. Rabeau, S. Prawer, F. Jelezko, I. Mirza, J. Wrachtrup, *Nano Lett.* 7 (11) (2007) 3433–3437.
- [4] Y.R. Chang, H.Y. Lee, K. Chen, C.C. Chang, D.S. Tsai, C.C. Fu, T.S. Lim, Y.K. Tzeng, C.Y. Fang, C.C. Han, H.C. Chang, W. Fann, *Nat. Nanotechnol.* 3 (5) (2008) 284–288.
- [5] O.A. Williams, O. Douheret, M. Daenen, K. Haenen, E. Osawa, M. Takahashi, *Chemical Physics Letters* 445 (4–6) (2007) 255–258.
- [6] V.V. Danilenko, *Physics of the Solid State* 46 (4) (2004) 595–599.
- [7] O.A. Williams, J. Hees, C. Dieker, W. Jager, L. Kirste, C.E. Nebel, *ACS Nano* 4 (8) (2010) 4824–4830.
- [8] A. Kruger, F. Kataoka, M. Ozawa, T. Fujino, Y. Suzuki, A.E. Aleksenskii, A.Y. Vul', E. Osawa, *Carbon* 43 (8) (2005) 1722–1730.
- [9] S. Osswald, G. Yushin, V. Mochalin, S.O. Kucheyev, Y. Gogotsi, *J. Am. Chem. Soc.* 128 (35) (2006) 11635–11642.
- [10] J.E. Dahl, S.G. Liu, R.M.K. Carlson, *Science* 299 (5603) (2003) 96–99.
- [11] V.V. Danilenko, *Combustion, Explosion, and Shock Waves* 41 (4) (2005) 460–466.
- [12] I.I. Kulakova, *Physics of the Solid State* 46 (4) (2004) 636–643.
- [13] O.A. Shenderova, V.V. Zhirnov, D.W. Brenner, *Critical Reviews in Solid State and Materials Sciences* 27 (3–4) (2002) 227–356.
- [14] P. Badziag, W.S. Verwoerd, W.P. Ellis, N.R. Greiner, *Nature* 343 (6255) (1990) 244–245.

- [15] J.P. Boudou, P.A. Curmi, F. Jelezko, J. Wrachtrup, P. Aubert, M. Sennour, G. Balasubramanian, R. Reuter, A. Thorel, E. Gaffet, *Nanotechnology* 20 (23) (2009) 235602.
- [16] O.A. Williams, M. Nesladek, M. Daenen, S. Michaelson, A. Hoffman, E. Osawa, K. Haenen, R.B. Jackman, *Diamond & Related Materials* 17 (2008) 1080.
- [17] D.M. Gruen, *Mrs Bulletin* 26 (10) (2001) 771–776.
- [18] O.A. Williams, M. Daenen, J. D'Haen, K. Haenen, J. Maes, V.V. Moshchalkov, M. Nesladek, D.M. Gruen, *Diamond and Related Materials* 15 (2006) 654–658.
- [19] K. Ohtsuka, K. Suzuki, A. Sawabe, T. Inuzuka, *Japanese Journal of Applied Physics Part 2—Letters* 35 (8B) (1996) L1072–L1074.
- [20] W.S. Yang, J.H. Je, *Journal of Materials Research* 11 (7) (1996) 1787–1794.
- [21] M.A. Prelas, G. Popovici, L.K. Bigelow, *Handbook of Industrial Diamonds and Diamond Films*, Marcel Dekker Inc, New York, 1998, p. 1214.
- [22] X. Jiang, K. Schifffmann, C.P. Klages, *Physical Review B* 50 (12) (1994) 8402–8410.
- [23] J.L. Robins, *Applied Surface Science* 33–4 (1988) 379–394.
- [24] C.P. Chang, D.L. Flamm, D.E. Ibbotson, J.A. Mucha, *Journal of Applied Physics* 63 (5) (1988) 1744–1748.
- [25] B.V. Spitsyn, L.L. Bouilov, B.V. Derjaguin, *Journal of Crystal Growth* 52 (APR) (1981) 219–226.
- [26] K. Suzuki, A. Sawabe, H. Yasuda, T. Inuzuka, *Applied Physics Letters* 50 (12) (1987) 728–729.
- [27] P.A. Dennig, D.A. Stevenson, *Applied Physics Letters* 59 (13) (1991) 1562–1564.
- [28] P. Ascarelli, S. Fontana, *Applied Surface Science* 64 (4) (1993) 307–311.
- [29] M. Daenen, O.A. Williams, J. D'Haen, K. Haenen, M. Nesladek, *Physica Status Solidi A—Applications and Materials Science* 203 (12) (2006) 3005–3010.
- [30] S. Iijima, Y. Aikawa, K. Baba, *Applied Physics Letters* 57 (25) (1990) 2646–2648.
- [31] R. Akhvediani, I. Lior, S. Michaelson, A. Hoffman, *Diamond and Related Materials* 11 (3–6) (2002) 545–549.
- [32] K.V. Ravi, C.A. Koch, *Applied Physics Letters* 57 (4) (1990) 348–350.
- [33] A.A. Morrish, P.E. Pehrsson, *Applied Physics Letters* 59 (4) (1991) 417–419.
- [34] P.E. Pehrsson, J. Glesener, A. Morrish, *Thin Solid Films* 212 (1–2) (1992) 81–90.
- [35] B.E. Williams, J.T. Glass, *Journal of Materials Research* 4 (2) (1989) 373–384.
- [36] S.D. Wolter, J.T. Glass, B.R. Stoner, *Journal of Applied Physics* 77 (10) (1995) 5119–5124.
- [37] Z. Feng, M.A. Brewer, K. Komvopoulos, I.G. Brown, D.B. Bogy, *Journal of Materials Research* 10 (1) (1995) 165–174.
- [38] S. Yugo, T. Kanai, T. Kimura, T. Muto, *Applied Physics Letters* 58 (10) (1991) 1036–1038.
- [39] S. Yugo, T. Kimura, T. Muto, *Vacuum* 41 (4–6) (1990) 1364–1367.
- [40] B.R. Stoner, G.H.M. Ma, S.D. Wolter, J.T. Glass, *Physical Review B* 45 (19) (1992) 11067–11084.
- [41] X. Jiang, C.P. Klages, *Diamond and Related Materials* 2 (5–7) (1993) 1112–1113.
- [42] W. Zhu, F.R. Sivazlian, B.R. Stoner, J.T. Glass, *Journal of Materials Research* 10 (2) (1995) 425–430.
- [43] A. Sawabe, T. Inuzuka, *Applied Physics Letters* 46 (2) (1985) 146–147.
- [44] J. Robertson, *Diamond and Related Materials* 4 (5–6) (1995) 549–552.
- [45] Y. Lifshitz, T. Kohler, T. Frauenheim, I. Guzman, A. Hoffman, R.Q. Zhang, X.T. Zhou, S.T. Lee, *Science* 297 (5586) (2002) 1531–1533.
- [46] J.C. Arnault, S. Saada, S. Delclos, L. Rocha, L. Intiso, R. Polini, A. Hoffman, S. Michaelson, P. Bergonzo, *Chemical Vapor Deposition* 14 (7–8) (2008) 187–195.
- [47] M.W. Geis, *Applied Physics Letters* 55 (6) (1989) 550–552.
- [48] J. Philip, P. Hess, T. Feygelson, J.E. Butler, S. Chattopadhyay, K.H. Chen, L.C. Chen, *Journal of Applied Physics* 93 (4) (2003) 2164–2171.
- [49] H.A. Girard, J.C. Arnault, S. Perruchas, S. Saada, T. Gacoin, J.P. Boilot, P. Bergonzo, *Diamond and Related Materials* 19 (7) (2010) 1117–1123.
- [50] E. Scorsone, S. Saada, J.C. Arnault, P. Bergonzo, *Journal of Applied Physics* 106 (1) (2009) 014908.
- [51] M. Daenen, L. Zhang, R. Erni, O.A. Williams, A. Hardy, M.K. Van Bael, P. Wagner, K. Haenen, M. Nesladek, G. Van Tendeloo, *Advanced Materials* 21 (6) (2009) 670.
- [52] H.A. Girard, S. Perruchas, C. Gesset, M. Chaigneau, L. Vieille, J.C. Arnault, P. Bergonzo, J.P. Boilot, T. Gacoin, *ACS Applied Materials & Interfaces* 1 (12) (2009) 2738–2746.
- [53] K. Tsugawa, M. Ishihara, J. Kim, Y. Koga, M. Hasegawa, *Journal of Physical Chemistry C* 114 (9) (2010) 3822–3824.
- [54] A. Giraud, T. Jenny, E. Leroy, O.M. Küttel, L. Schlapbach, P. Vanelle, L. Giraud, *Journal of the American Chemical Society* 123 (10) (2001) 2271–2274.
- [55] L. Giraud, V. Huber, T. Jenny, *Tetrahedron* 54 (39) (1998) 11899–11906.
- [56] E. Leroy, O.M. Küttel, L. Schlapbach, L. Giraud, T. Jenny, *Applied Physics Letters* 73 (8) (1998) 1050–1052.
- [57] N.N. Naguib, J.W. Elam, J. Birrell, J. Wang, D.S. Grierson, B. Kabius, J.M. Hiller, A.V. Sumant, R.W. Carpick, O. Auciello, J.A. Carlisle, *Chemical Physics Letters* 430 (4–6) (2006) 345–350.
- [58] S.Z. Rotter, J.C. Madaleno, *Chemical Vapor Deposition* 15 (7–9) (2009) 209–216.
- [59] A.V. Sumant, P. Gilbert, D.S. Grierson, A.R. Konicek, M. Abrecht, J.E. Butler, T. Feygelson, S.S. Rotter, R.W. Carpick, *Diamond & Related Materials* 16 (2007) 718–724.
- [60] J.J. Lee, W.S. Yang, J.H. Je, *Journal of Materials Research* 12 (3) (1997) 657–664.
- [61] J.C. Arnault, S. Saada, M. Nesladek, O.A. Williams, K. Haenen, P. Bergonzo, E. Osawa, *Diamond and Related Materials* 17 (7–10) (2008) 1143–1149.
- [62] O.A. Williams, M. Daenen, J. D'Haen, K. Haenen, J. Maes, V.V. Moshchalkov, M. Nesladek, D.M. Gruen, *Diamond and Related Materials* 15 (4–8) (2006) 654–658.
- [63] A. Van Der Drift, *Philips Research Report* 22 (1967) 267.
- [64] P. Achatz, J.A. Garrido, M. Stutzmann, O.A. Williams, D.M. Gruen, A. Kromka, D. Steinmuller, *Applied Physics Letters* 88 (10) (2006) 101908.
- [65] P. Achatz, J.A. Garrido, O.A. Williams, P. Brun, D.M. Gruen, A. Kromka, D. Steinmuller, M. Stutzmann, *Physica Status Solidi A—Applications and Materials Science* 204 (9) (2007) 2874–2880.
- [66] O.A. Williams, *Semiconductor Science and Technology* 21 (8) (2006) R49–R56.
- [67] O.A. Williams, M. Nesladek, *Physica Status Solidi A—Applications and Materials Science* 203 (13) (2006) 3375–3386.
- [68] O.A. Williams, M. Nesladek, M. Daenen, S. Michaelson, A. Hoffman, E. Osawa, K. Haenen, R.B. Jackman, *Diamond and Related Materials* 17 (7–10) (2008) 1080–1088.
- [69] W. Müller-Sebert, C. Wild, P. Koidl, N. Herres, J. Wagner, T. Eckermann, *Materials Science and Engineering: B* 11 (1–4) (1992) 173–178.
- [70] D.M. Gruen, *Annual Review of Materials Science* 29 (1999) 211–259.
- [71] K. Subramanian, W.P. Kang, J.L. Davidson, W.H. Hofmeister, J. Vac. Sci. Technol. B 23 (2) (2005) 786–792.
- [72] D.T. Tran, W.S. Huang, J. Asmussen, T.A. Grotjohn, D.K. Reinhard, *New Diamond and Frontier Carbon Technology* 16 (6) (2006) 281–294.
- [73] O.A. Williams, A. Kriele, J. Hees, M. Wolfer, W. Muller-Sebert, C.E. Nebel, *Chemical Physics Letters* 495 (1–3) (2010) 84–89.
- [74] R. Haubner, B. Lux, *International Journal of Refractory Metals and Hard Materials* 20 (2) (2002) 93–100.
- [75] S. Jiao, A. Sumant, M.A. Kirk, D.M. Gruen, A.R. Krauss, O. Auciello, *Journal of Applied Physics* 90 (1) (2001) 118–122.
- [76] S. Saada, J.C. Arnault, L. Rocha, B. Bazin, P. Bergonzo, *Physica Status Solidi A—Applications and Materials Science* 205 (9) (2008) 2121–2125.
- [77] F.J.H. Guillen, K. Janischowsky, W. Ebert, E. Kohn, *Physica Status Solidi A—Applied Research* 201 (11) (2004) 2553–2557.
- [78] F.J.H. Guillen, K. Janischowsky, J. Kusterer, W. Ebert, E. Kohn, *Diamond and Related Materials* 14 (3–7) (2005) 411–415.
- [79] D. Schwarzbach, R. Haubner, B. Lux, *Diamond and Related Materials* 3 (4–6) (1994) 757–764.
- [80] L.C. Nistor, J. Van Landuyt, V.G. Ralchenko, E.D. Obraztsova, A.A. Smolin, *Diamond and Related Materials* 6 (1) (1997) 159–168.
- [81] K. Tsugawa, M. Ishihara, J. Kim, M. Hasegawa, Y. Koga, *New Diam. Front. C. Tec.* 16 (6) (2006) 337–346.
- [82] T.H. Metcalf, X. Liu, B.H. Houston, J.W. Baldwin, J.E. Butler, T. Feygelson, *Applied Physics Letters* 86 (8) (2005) 081910.
- [83] L. Sekaric, J.M. Parpia, H.G. Craighead, T. Feygelson, B.H. Houston, J.E. Butler, *Applied Physics Letters* 81 (23) (2002) 4455–4457.
- [84] O.A. Williams, S. Curat, J.E. Gerbi, D.M. Gruen, R.B. Jackman, *Applied Physics Letters* 85 (10) (2004) 1680–1682.
- [85] R. Haubner, B. Lux, *Diamond and Related Materials* 2 (9) (1993) 1277–1294.
- [86] A. Sawabe, T. Inuzuka, *Thin Solid Films* 137 (1) (1986) 89–99.
- [87] K. Suzuki, A. Sawabe, T. Inuzuka, *Japanese Journal of Applied Physics Part 1—Regular Papers Short Notes & Review Papers* 29 (1) (1990) 153–157.
- [88] M.A. Prelas, G. Popovici, L.K. Bigelow, *Handbook of Industrial Diamonds and Diamond Films*, Marcel Dekker, New York, 1998, xii, 1214 pp.
- [89] J.E. Butler, R.L. Woodin, *Philosophical Transactions of the Royal Society of London Series A—Mathematical Physical and Engineering Sciences* 342 (1664) (1993) 209–224.
- [90] D.G. Goodwin, J.E. Butler, *Handbook of Industrial Diamonds and Diamond Films*, Marcel Dekker, New York, 1998, pp. 527–581.
- [91] J.E. Butler, Y.A. Mankelevich, A. Cheesman, J. Ma, M.N.R. Ashfold, *Journal of Physics—Condensed Matter* 21 (36) (2009) 364201.
- [92] F.G. Celii, P.E. Pehrsson, H.T. Wang, J.E. Butler, *Applied Physics Letters* 52 (24) (1988) 2043–2045.
- [93] M.N.R. Ashfold, P.W. May, J.R. Petherbridge, K.N. Rosser, J.A. Smith, Y.A. Mankelevich, N.V. Suetin, *Physical Chemistry Chemical Physics* 3 (17) (2001) 3471–3485.
- [94] D.M. Gruen, C.D. Zuiker, A.R. Krauss, X.Z. Pan, *Journal of Vacuum Science & Technology A—Vacuum Surfaces and Films* 13 (3) (1995) 1628–1632.
- [95] A.N. Goyette, J.E. Lawler, L.W. Anderson, D.M. Gruen, T.G. McCauley, D. Zhou, A.R. Krauss, *Journal of Physics D—Applied Physics* 31 (16) (1998) 1975–1986.
- [96] M. Eckert, E. Neyts, A. Bogaerts, *Chemical Vapor Deposition* 14 (7–8) (2008) 213–223.
- [97] J.R. Rabeau, P. John, J.I.B. Wilson, Y. Fan, *Journal of Applied Physics* 96 (11) (2004) 6724.
- [98] S. Saada, S. Pochet, L. Rocha, J.C. Arnault, P. Bergonzo, *Diamond and Related Materials* 18 (5–8) (2009) 707–712.
- [99] J.C. Lee, B.Y. Hong, R. Messier, R.W. Collins, *Applied Physics Letters* 69 (12) (1996) 1716–1718.
- [100] A. Zimmer, O.A. Williams, K. Haenen, H. Terryn, *Applied Physics Letters* 93 (13) (2008) 131910.
- [101] B. Hong, J. Lee, R.W. Collins, Y. Kuang, W. Drawl, R. Messier, T.T. Tsong, Y.E. Strausser, *Diamond and Related Materials* 6 (1) (1997) 55–80.
- [102] M. Lions, S. Saada, J.P. Mazellier, F. Andrieu, O. Faynot, P. Bergonzo, *Physica Status Solidi—Rapid Research Letters* 3 (6) (2009) 205–207.
- [103] A. Kriele, O.A. Williams, M. Wolfer, D. Brink, W. Muller-Sebert, C.E. Nebel, *Applied Physics Letters* 95 (3) (2009) 031905.
- [104] S. Michaelson, A. Stacey, J. Orwa, A. Cimmino, S. Prawer, B.C.C. Cowie, O.A. Williams, D.M. Gruen, A. Hoffman, *Journal of Applied Physics* 107 (9) (2010) 093521.
- [105] S. Michaelson, O. TERNYAK, R. Akhvediani, A. Hoffmann, A. Lafosse, R. Azria, O.A. Williams, D.M. Gruen, *Journal of Applied Physics* 102 (11) (2007) 113516.
- [106] S. Michaelson, O. TERNYAK, R. Akhvediani, O.A. Williams, D. Gruen, A. Hoffman, *Physica Status Solidi A—Applications and Materials Science* 204 (9) (2007) 2860–2867.
- [107] S. Michaelson, O. TERNYAK, A. Hoffman, O.A. Williams, D.M. Gruen, *Applied Physics Letters* 91 (10) (2007) 103104.
- [108] S. Osswald, V.N. Mochalin, M. Havel, G. Yushin, Y. Gogotsi, *Physical Review B* 80 (7) (2009).

- [109] A.C. Ferrari, J. Robertson, *Physical Review B* 61 (20) (2000) 14095–14107.
- [110] S. Praver, K.W. Nugent, D.N. Jamieson, J.O. Orwa, L.A. Bursill, J.L. Peng, *Chem. Phys. Lett.* 332 (2000) 93–97.
- [111] A.C. Ferrari, J. Robertson, *Physical Review B* 63 (12) (2001) 121405.
- [112] H. Kuzmany, R. Pfeiffer, N. Salk, B. Gunther, *Carbon* 42 (5–6) (2004) 911–917.
- [113] R. Pfeiffer, H. Kuzmany, P. Knoll, S. Bokova, N. Salk, B. Gunther, *Diam. Relat. Mater.* 12 (2003) 268–271.
- [114] R. Pfeiffer, H. Kuzmany, N. Salk, B. Gunther, *Applied Physics Letters* 82 (23) (2003) 4149–4150.
- [115] D. Zhou, D.M. Gruen, L.C. Qin, T.G. McCauley, A.R. Krauss, *Journal of Applied Physics* 84 (4) (1998) 1981–1989.
- [116] S. Bühlmann, E. Blank, R. Haubner, B. Lux, *Diamond and Related Materials* 8 (2–5) (1999) 194–201.
- [117] B. Watts, L. Thomsen, P.C. Dastoor, *Journal of Electron Spectroscopy and Related Phenomena* 15 (2) (2006) 105–120.
- [118] J.F. Morar, F.J. Himpel, G. Hollinger, J.L. Jordon, G. Hughes, F.R. Mcfeely, *Physical Review B* 33 (2) (1986) 1346–1349.
- [119] T.W. Capelhart, T.A. Perry, C.B. Beetz, D.N. Belton, G.B. Fisher, C.E. Beall, B.N. Yates, J.W. Taylor, *Applied Physics Letters* 55 (10) (1989) 957–959.
- [120] F.L. Coffman, R. Cao, P.A. Pianetta, S. Kapoor, M. Kelly, L.J. Terminello, *Applied Physics Letters* 69 (4) (1996) 568–570.
- [121] C.J. Chu, R.H. Hauge, J.L. Margrave, M.P. Develyn, *Applied Physics Letters* 61 (12) (1992) 1393–1395.
- [122] X. Xiao, J. Birrell, J.E. Gerbi, O. Auciello, J.A. Carlisle, *Journal of Applied Physics* 96 (4) (2004) 2232–2239.
- [123] A.V. Sumant, O. Auciello, R.W. Carpick, S. Srinivasan, J.E. Butler, *Mrs Bulletin* 35 (4) (2010) 281–288.
- [124] S. Potocky, A. Kromka, J. Potmesil, Z. Remes, V. Vorlicek, M. Vanecek, M. Michalka, *Diamond and Related Materials* 16 (4–7) (2007) 744–747.
- [125] C.J. Morath, H.J. Maris, J.J. Cuomo, D.L. Pappas, A. Grill, V.V. Patel, J.P. Doyle, K.L. Saenger, *Journal of Applied Physics* 76 (5) (1994) 2636–2640.
- [126] M. Imboden, P. Mohanty, *Physical Review B* 79 (12) (2009) 125424.
- [127] P. Achatz, E. Bustarret, C. Marcenat, R. Piqueret, T. Dubouchet, C. Chapelier, A.M. Bonnot, O.A. Williams, K. Haenen, W. Gajewski, J.A. Garrido, M. Stutzmann, *Physica Status Solidi A—Applications and Materials Science* 206 (9) (2009) 1978–1985.
- [128] P. Achatz, W. Gajewski, E. Bustarret, C. Marcenat, R. Piqueret, C. Chapelier, T. Dubouchet, O.A. Williams, K. Haenen, J.A. Garrido, M. Stutzmann, *Physical Review B* 79 (20) (2009) 201203.
- [129] F. Dahlem, P. Achatz, O.A. Williams, D. Araujo, E. Bustarret, H. Courtois, *Physical Review B* 82 (3) (2010) 033306.
- [130] M.P. Villar, M.P. Alegre, D. Araujo, E. Bustarret, P. Achatz, L. Saminadaya, C. Bauerle, O.A. Williams, *Physica Status Solidi A—Applications and Materials Science* 206 (9) (2009) 1986–1990.
- [131] S. Bhattacharyya, O. Auciello, J. Birrell, J.A. Carlisle, L.A. Curtiss, A.N. Goyette, D.M. Gruen, A.R. Krauss, J. Schlueter, A. Sumant, P. Zapol, *Applied Physics Letters* 79 (10) (2001) 1441–1443.
- [132] J. Birrell, J.A. Carlisle, O. Auciello, D.M. Gruen, J.M. Gibson, *Applied Physics Letters* 81 (12) (2002) 2235–2237.
- [133] J. Birrell, J.E. Gerbi, O. Auciello, J.M. Gibson, D.M. Gruen, J.A. Carlisle, *Journal of Applied Physics* 93 (9) (2003) 5606–5612.
- [134] M. Nesladek, K. Meykens, L.M. Stals, M. Vanecek, J. Rosa, *Physical Review B* 54 (8) (1996) 5552–5561.
- [135] C. Arena, B. Kleinsorge, J. Robertson, W.I. Milne, M.E. Welland, *Journal of Applied Physics* 85 (3) (1999) 1609–1615.
- [136] M.J. Tadjer, K.D. Hobart, J.D. Caldwell, J.E. Butler, K.X. Liu, C.R. Eddy, D.K. Gaskill, K.K. Lew, B.L. Vanmil, R.L. Myers-Ward, M.G. Ancona, F.J. Kub, T.I. Feygelson, *Applied Physics Letters* 91 (16) (2007).
- [137] M.J. Tadjer, K.D. Hobart, J.D. Caldwell, M.A. Mastro, T.I. Feygelson, J.E. Butler, D.A. Alexson, F.J. Kub, I. Lee, *Investigation of Nanocrystalline Diamond Films as UV Transparent Ohmic Contacts to GaN, International Semiconductor Device Research Symposium, 2007., College Pk, MD.*
- [138] T. Zimmermann, M. Kubovic, A. Denisenko, K. Janischowsky, O.A. Williams, D.M. Gruen, E. Kohn, *Diamond and Related Materials* 14 (3–7) (2005) 416–420.
- [139] G. Chandler, J. Zimmer, I. Lee, *Enhancing SOI with Thin Film Diamond, 2008 IEEE International SOI Conference, Proceedings, 2008, pp. 101–102.*
- [140] M. Rabarot, J. Wdziez, S. Saada, J.P. Mazellier, C. Lecouvey, J.C. Roussin, J. Dechamp, P. Bergonzo, F. Andrieu, O. Faynot, S. Deleonibus, L. Clavelier, J.P. Roger, *Diamond and Related Materials* 19 (7–9) (2010) 796–805.
- [141] K. Raleva, D. Vasileska, S.M. Goodnick, *IEEE Electron Device Letters* 29 (6) (2008) 621–624.
- [142] A. Aleksov, X. Li, N. Govindaraju, J.M. Gobien, S.D. Wolter, J.T. Prater, Z. Sitar, *Diamond and Related Materials* 14 (3–7) (2005) 308–313.
- [143] A. Erdemir, G.R. Fenske, A.R. Krauss, D.M. Gruen, T. McCauley, R.T. Csencsits, *Surface & Coatings Technology* 121 (1999) 565–572.
- [144] A.R. Krauss, O. Auciello, D.M. Gruen, A. Jayatissa, A. Sumant, J. Tucek, D.C. Mancini, N. Moldovan, A. Erdemir, D. Ersoy, M.N. Gardos, H.G. Busmann, E.M. Meyer, M.Q. Ding, *Diamond and Related Materials* 10 (11) (2001) 1952–1961.
- [145] A. Gaidarzhly, M. Imboden, P. Mohanty, J. Rankin, B.W. Sheldon, *Applied Physics Letters* 91 (20) (2007), p. -.
- [146] M. Imboden, P. Mohanty, A. Gaidarzhly, J. Rankin, B.W. Sheldon, *Applied Physics Letters* 90 (17) (2007), p. -.
- [147] M.A. Huff, D.A. Aidala, J.E. Butler, *Solid State Technology* 49 (4) (2006) 45–+.
- [148] A.B. Hutchinson, P.A. Truitt, K.C. Schwab, L. Sekaric, J.M. Parpia, H.G. Craighead, J.E. Butler, *Applied Physics Letters* 84 (6) (2004) 972–974.
- [149] E. Sillero, O.A. Williams, V. Lebedev, V. Cimalla, C.C. Rohlig, C.E. Nebel, F. Calle, *Journal of Micromechanics and Microengineering* 19 (11) (2009) 115016.
- [150] F.J. Hernández Guillén, K. Janischowsky, J. Kusterer, W. Ebert, E. Kohn, *Diamond and Related Materials* 14 (3–7) (2005) 411–415.
- [151] E. Kohn, P. Gluche, M. Adamschik, *Diamond and Related Materials* 8 (2–5) (1999) 934–940.
- [152] S. Mandal, C. Naud, O.A. Williams, E. Bustarret, F. Omnes, P. Rodiere, T. Meunier, L. Saminadaya, C. Bauerle, *Nanotechnology* 21 (19) (2010).
- [153] E. Kohn, M. Adamschik, P. Schmid, S. Ertl, A. Floter, *Diamond and Related Materials* 10 (9–10) (2001) 1684–1691.
- [154] J. Wang, J.E. Butler, T. Feygelson, C.T.C. Nguyen, I. Lee, *1.51-GHz Nanocrystalline Diamond Micromechanical Disk Resonator with Material-mismatched Isolating Support, MEMS 2004: 17th IEEE International Conference on Micro Electro Mechanical Systems, Technical Digest, 2004.*
- [155] J.W. Baldwin, M.K. Zalalutdinov, T. Feygelson, B.B. Pate, J.E. Butler, B.H. Houston, *Diamond and Related Materials* 15 (11–12) (2006) 2061–2067.
- [156] C.F. Wang, R. Hanson, D.D. Awschalom, E.L. Hu, T. Feygelson, J. Yang, J.E. Butler, *Applied Physics Letters* 91 (20) (2007) 201112.
- [157] C.F. Wang, Y.S. Choi, J.C. Lee, E.L. Hu, J. Yang, J.E. Butler, *Applied Physics Letters* 90 (8) (2007) 81110.
- [158] O.A. Williams, V. Mortet, M. Daenen, K. Haenen, *Applied Physics Letters* 90 (6) (2007) 063514.
- [159] O.A. Williams, V. Mortet, M. Daenen, K. Haenen, *Journal of Nanoscience and Nanotechnology* 9 (6) (2009) 3483–3486.
- [160] S. Srinivasan, J. Hiller, B. Kabius, O. Auciello, *Applied Physics Letters* 90 (13) (2007), p. -.
- [161] R. Abdolvand, G.K. Ho, J. Butler, F. Ayazi, I. Lee, *ZnO-on-nanocrystalline Diamond Lateral Bulk Acoustic Resonators, Proceedings of the IEEE Twentieth Annual International Conference on Micro Electro Mechanical Systems, Vols 1 and 2, 2007, pp. 686–689.*
- [162] A. Hikavy, P. Clauws, K. Vanbesien, P. De Visschere, O.A. Williams, M. Daenen, K. Haenen, J.E. Butler, T. Feygelson, *Diamond and Related Materials* 16 (4–7) (2007) 983–986.
- [163] F. Benedic, M.B. Assouar, P. Kirsch, D. Moneger, O. Brinza, O. Elmazria, P. Alnot, A. Ciccuel, *Diamond and Related Materials* 17 (4–5) (2008) 804–808.
- [164] E. Chevallier, E. Scorsone, P. Bergonzo, *Modified Diamond Nanoparticles as Sensitive Coatings for Chemical SAW Sensors, in: J. Brugger, D. Briand (Eds.), Proceedings of the Eurosensors XXIII Conference, 2009, pp. 943–946.*
- [165] V. Mortet, O.A. Williams, K. Haenen, *Physica Status Solidi A—Applications and Materials Science* 205 (5) (2008) 1009–1020.
- [166] H.B. Martin, A. Argoitia, U. Landau, A.B. Anderson, J.C. Angus, *Journal of the Electrochemical Society* 143 (6) (1996) L133–L136.
- [167] M. Hupert, A. Muck, R. Wang, J. Stotter, Z. Cvackova, S. Haymond, Y. Show, G.M. Swain, *Diamond and Related Materials* 12 (10–11) (2003) 1940–1949.
- [168] J.K. Zak, J.E. Butler, G.M. Swain, *Analytical Chemistry* 73 (5) (2001) 908–914.
- [169] J. Stotter, Y. Show, S.H. Wang, G. Swain, *Chemistry of Materials* 17 (19) (2005) 4880–4888.
- [170] J. Stotter, J. Zak, Z. Behier, Y. Show, G.M. Swain, *Analytical Chemistry* 74 (23) (2002) 5924–5930.
- [171] N. Smisdom, I. Smets, O.A. Williams, M. Daenen, S. Wenmackers, K. Haenen, M. Nesladek, J. D'Haen, P. Wagner, J.M. Rigo, M. Ameloot, M. Vandeven, *Physica Status Solidi A—Applications and Materials Science* 206 (9) (2009) 2042–2047.
- [172] C.G. Specht, O.A. Williams, R.B. Jackman, R. Schoepfer, *Biomaterials* 25 (18) (2004) 4073–4078.
- [173] M. Bonnauron, S. Saada, C. Mer, C. Gesset, O.A. Williams, L. Rousseau, E. Scorsone, P. Mailley, M. Nesladek, J.C. Arnault, P. Bergonzo, *Physica Status Solidi A—Applications and Materials Science* 205 (9) (2008) 2126–2129.
- [174] G.M. Swain, J.M. Stotter, S. Haymond, Y. Show, J.K. Zak, *Abstracts of Papers of the American Chemical Society* 225 (2003) U690–U691.
- [175] J. Hernandez, T. Pourrostami, J.A. Garrido, O.A. Williams, D.M. Gruen, A. Kromka, D. Steinmuller, M. Stutzmann, *Diamond and Related Materials* 16 (1) (2007) 138–143.
- [176] J.L. Davidson, W.P. Kang, A. Wisitsora-At, *Diamond and Related Materials* 12 (3–7) (2003) 429–433.
- [177] S. Bühlmann, E. Blank, R. Haubner, B. Lux, *Diamond and Related Materials* 8 (2–5) (1999) 194–201.
- [178] Q. Yang, S. Yang, Y.S. Li, X. Lu, A. Hirose, *Diamond and Related Materials* 16 (4–7) (2007) 730–734.
- [179] D.M. Gruen, A.R. Krauss, C.D. Zuiker, R. Csencsits, L.J. Terminello, J.A. Carlisle, I. Jimenez, D.G.J. Sutherland, D.K. Shuh, W. Tong, F.J. Himpel, *Applied Physics Letters* 68 (12) (1996) 1640–1642.
- [180] M.A. Angadi, T. Watanabe, A. Bodapati, X.C. Xiao, O. Auciello, J.A. Carlisle, J.A. Eastman, P. Keblinski, P.K. Schelling, S.R. Phillpot, *Journal of Applied Physics* 99 (11) (2006) 114301.
- [181] A. Heiman, I. Gouzman, S.H. Christiansen, H.P. Strunk, G. Comtet, L. Hellner, G. Dujardin, R. Edrei, A. Hoffman, *J. Appl. Phys.* 89 (5) (2001) 2622–2630.
- [182] T. Lin, G.Y. Yu, A.T.S. Wee, Z.X. Shen, K.P. Loh, *Applied Physics Letters* 77 (17) (2000) 2692–2694.
- [183] Y.F. Zhang, F. Zhang, Q.J. Gao, X.F. Peng, Z.D. Lin, *Diamond and Related Materials* 10 (8) (2001) 1523–1527.
- [184] J. Zhang, J.W. Zimmer, R.T. Howe, R. Maboudian, *Diamond and Related Materials* 17 (1) (2008) 23–28.